

RESEARCH ARTICLE

Impact of stabilizing mutations on the antigenic profile and glycosylation of membrane-expressed HIV-1 envelope glycoprotein

Tommy Tong¹, Alessio D'Addabbo², Jiamin Xu¹, Himanshi Chawla², Albert Nguyen¹, Paola Ochoa¹, Max Crispin², James M. Binley^{1*}

1 San Diego Biomedical Research Institute, San Diego, California, United States of America, **2** School of Biological Sciences, University of Southampton, Southampton, United Kingdom

* jbinley@sdbri.org



Abstract

Recent HIV-1 vaccine development has centered on “near native” soluble envelope glycoprotein (Env) trimers that are artificially stabilized laterally (between protomers) and apically (between gp120 and gp41). These mutations have been leveraged for use in membrane-expressed Env mRNA vaccines, although their effects in this context are unclear. To address this question, we used virus-like particle (VLP) produced in 293T cells. Uncleaved (UNC) trimers were laterally unstable upon gentle lysis from membranes. However, gp120/gp41 processing improved lateral stability. Due to inefficient gp120/gp41 processing, UNC is incorporated into VLPs. A linker between gp120 and gp41 neither improved trimer stability nor its antigenic profile. An artificially introduced enterokinase cleavage site allowed post-expression gp120/gp41 processing, concomitantly increasing trimer stability. Gp41 N-helix mutations I559P and NT1-5 imparted lateral trimer stability, but also reduced gp120/gp41 processing and/or impacted V2 apex and interface NAb binding. I559P consistently reduced recognition by HIV+ human plasmas, further supporting antigenic differences. Mutations in the gp120 bridging sheet failed to stabilize membrane trimers in a pre-fusion conformation, and also reduced gp120/gp41 processing and exposed non-neutralizing epitopes. Reduced glycan maturation and increased sequon skipping were common side effects of these mutations. In some cases, this may be due to increased rigidity which limits access to glycan processing enzymes. In contrast, viral gp120 did not show glycan skipping. A second, minor species of high mannose gp160 was unaffected by any mutations and instead bypasses normal folding and glycan maturation. Including the full gp41 cytoplasmic tail led to markedly reduced gp120/gp41 processing and greatly increased the proportion of high mannose gp160. Remarkably, monoclonal antibodies were unable to bind to this high mannose gp160 in native protein gels. Overall, our findings suggest caution in leveraging stabilizing mutations in nucleic acid-based immunogens to ensure they impart valuable membrane trimer phenotypes for vaccine use.

OPEN ACCESS

Citation: Tong T, D'Addabbo A, Xu J, Chawla H, Nguyen A, Ochoa P, et al. (2023) Impact of stabilizing mutations on the antigenic profile and glycosylation of membrane-expressed HIV-1 envelope glycoprotein. PLoS Pathog 19(8): e1011452. <https://doi.org/10.1371/journal.ppat.1011452>

Editor: Daniel C. Douek, Vaccine Research Center, UNITED STATES

Received: June 1, 2023

Accepted: July 16, 2023

Published: August 7, 2023

Copyright: © 2023 Tong et al. This is an open access article distributed under the terms of the [Creative Commons Attribution License](#), which permits unrestricted use, distribution, and reproduction in any medium, provided the original author and source are credited.

Data Availability Statement: Data are held in the manuscript and supporting files. Glycopeptide LC-MS data can be found in the MassIVE database, accession number: MSV000092416.

Funding: This work was supported by NIH grant AI93278 (JMB) and the International AIDS Vaccine Initiative (IAVI) grant INV-008352/OPP1153692 funded by the Bill and Melinda Gates Foundation (MC). The funders had no role in study design, data

collection and analysis, decision to publish, or preparation of the manuscript.

Competing interests: The authors have declared that no competing interests exist.

Author summary

A vaccine that induces virus-fighting antibodies to block HIV-1 infection remains elusive. To ablate HIV-1 infection, antibodies must bind to authentic envelope (Env) glycoprotein on the virus surface. However, Env can exist in various forms, many of which are relatively easy targets for non-effective antibodies. Therefore, a key challenge of vaccine design is to create pure authentic Env that is unfettered by these other forms of Env. Vaccine research to date has focused largely on stabilizing soluble Env trimers, as this format simplifies purification and translational studies. However, incomplete Env authenticity may blunt the efficacy of this approach. By comparison, the manufacture of particle-based vaccines that express Env *in situ* on membranes is cumbersome. In an alternative approach, lipid particles can deliver mRNA vaccines encoding membrane trimers, bypassing the manufacturing challenges of previous methods. Stabilizing mutations derived from soluble trimers are now being leveraged for membrane trimers. Here, we evaluated the effects of these mutations. Our results show that some mutations alter Env conformation, and therefore might best be omitted from nucleic acid-based membrane Env vaccines.

Introduction

HIV-1 envelope glycoprotein (Env) gp120/gp41 trimers are the natural target of broadly neutralizing antibodies (bNAbs). These trimers use sophisticated strategies to evade bNAbs, including high sequence variation of exposed surfaces, a dense glycan shield, low viral spike density and conformationally dynamic epitopes [1–4]. Env trimers can assume various conformations, ranging from fully open to the closed, pre-fusion state. Many bNAbs exhibit a preference for the pre-fusion state (termed “state 1”) [1,3], supporting efforts to present this form of Env in vaccines.

Mutational studies aimed at stabilizing soluble gp140 laid the groundwork for the first crystal structure of a “near native” trimer [5]. Gp140 was first stabilized apically via an “SOS” disulfide bond between gp120 and gp41 (A501C+T605C) [6], then laterally via a proline mutation in the N-helix of gp41 (I559P), collectively termed “SOSIP” gp140 [7]. I559P destabilizes the low energy post-fusion “6 helix bundle” conformation of transmembrane domains, so that the C-helices can self-associate. Alternatively, a linker also situated in the gp41 N-helix (AA548–568, termed UFO) lends lateral stability [8]. To address the challenge of incomplete cellular processing into gp120/gp41, one solution has been to introduce a linker, e.g., NFL (native flexibly linked), to provide gp120 and gp41 with flexibility to associate in a native-like manner [9,10].

Soluble trimer structures have revitalized vaccine research by providing a template for rational, mutation-based vaccine designs. For example, A433P and DS (I201C+A433C to cross-link the β3 and β21 strands of gp120) both prevent soluble trimers from adopting a CD4-induced state [11]. Other mutation strategies include: i) leveraging residues from strains that form well-folded gp140 trimers [12–20], ii) rendering trimers vulnerable to bNAb precursors [21,22], and iii) stabilizing the pre-fusion state by improving electrostatic interactions [23].

Vaccines that present authentic trimers in their natural, membrane context might be our best hope to elicit bNAbs. Accordingly, we have been developing virus-like particles (VLPs) expressing trimers as a vaccine platform [24–26]. Native trimers are generated from an uncleaved (UNC) gp160 precursor. The conformational flexibility of UNC gp160 is essential

for it to reach its mature form, facilitating glycan addition/maturation, disulfide isomerization until canonical disulfides form, followed by signal peptide removal and gp120/gp41 processing [27,28]. It is therefore not surprising that UNC exists in a variety of oligomeric states that are sensitive to non-NAbs [1,29–34].

To date, various membrane trimer mutants (SOS, I559P and UNC), like their soluble gp140 counterparts, mostly adopt relatively “open” trimer states 2 and 3, recognized by non-NAbs [3,35–42]. On the other hand, native membrane trimers, but not UNC, are exclusively bound by NAb [30,33,34]. Incomplete gp120/gp41 processing is a consistent unwanted feature of membrane Env expressed on VLPs, pseudovirions and even infectious molecular clones expressed in 293T cells [30,43–45]. Non-functional Env comes in a variety of forms. While some UNC gp160 acquires complex glycans, a fraction acquires only high mannose glycans in some cell lines, apparently bypassing normal glycosylation [32,34,39,46]. Furthermore, gp120 shedding leaves behind gp41 stumps [30].

mRNA vaccines have great potential to simplify the otherwise challenging translation of membrane-expressed trimer vaccine concepts into the clinic [47–50]. So far, data suggests that mRNA-expressing membrane trimers outperform soluble trimers [10,51–55]. Mutations that were previously used for soluble trimer vaccines have been leveraged in corresponding membrane trimers [51–54,56,57]. A phase I trial of 3 mRNA-based HIV vaccines is now underway (HVTN302), 2 of which express membrane Env and carry various mutations including SOS, I559P, NFL-like linker, cytoplasmic tail truncation, and mutations to improve antigenicity and thermal stability [58]. However, the effects of these stabilizing mutations may differ in the context of membrane trimers. While some mutations, for example SOS, are widely adaptable, others may have context-dependent effects [22]. The DS mutation may decrease gp120/gp41 processing of membrane trimers [36]. Similarly, the effects of I559P and UFO might differ for membrane trimers if they are already stable in a membrane context [10,30,38,53,59]. These challenges are compounded by the co-expression of non-functional Env isoforms [30]. This is important because mRNA expression cannot “filter out” non-functional Env that might dampen antibody responses away from the intended native trimer targets.

Previously, a panel of HIV Env mutants including SOS, I559P, A433P, DS, NFL, UFO, both alone and in combination, were evaluated antigenically using MAbs to down select lead constructs for mRNA delivery [10]. However, it remains unclear how these mutations impact stability, gp120/gp41 processing, expression, glycosylation and non-functional Env. To fill this knowledge gap and to identify valuable mutation(s) for future mRNA vaccine studies, we compared various mutants alone and in combination in the context of VLP-expressed membrane trimers. Our data suggest that different modifications variably impacted Env expression, gp120/gp41 processing, glycosylation, antigenicity, and stability in the lateral and apical planes. Our findings can assist in making informed modifications in membrane-expressed vaccine constructs.

Results

Expression and maturation of membrane trimer mutants

We typically make VLPs expressing SOS mutant Env because it eliminates gp120 shedding. In addition, we truncate the gp41 cytoplasmic tail (gp160 Δ CT) both to improve expression and gp120/gp41 processing [30]. The resulting mutant is measurably infectious and typically retains a tier 2 profile [30,60]. Other mutations can stabilize soluble gp140 trimers in a “closed” conformation resembling native spikes. These include deletions, linkers, engineered disulfides and proline substitutions. It remains unclear which of these modifications are needed for optimal NAb induction by mRNA vaccine-encoded Env *membrane* trimers [10,52–54]. To address

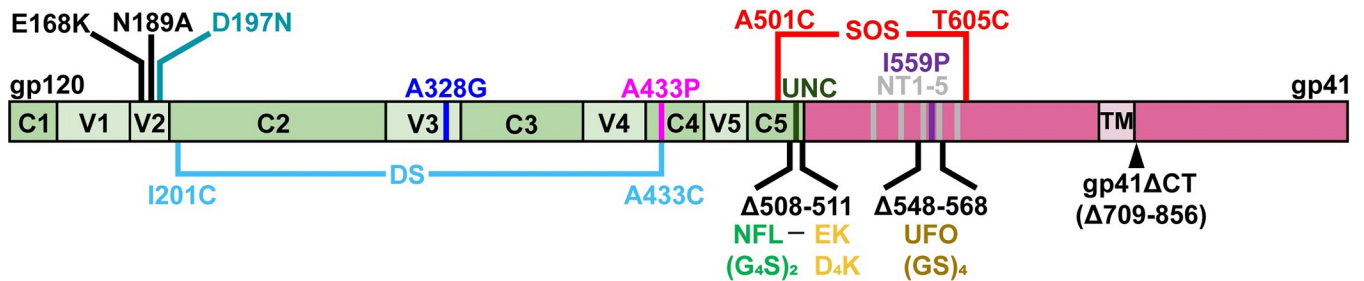


Fig 1. HIV-1 gp160 mutants. A schematic of gp160 showing gp120 (green) variable (V1-V5) domains, constant domains (C1-C5), and gp41 (salmon), including the transmembrane domain (TM). Mutants are shown in different colors that we also use consistently hereafter for clarity. Amino acids are numbered according to HxB2 subtype B reference strain. Gp41 was truncated from position 709 onwards, leaving three amino acids after the TM domain in gp160ΔCT. Most of our JR-FL mutants are based on gp160ΔCT SOS E168K+N189A, unless otherwise stated. NFL is “native flexibly linked” with Gly-Gly-Gly-Ser sequence repeated twice, which replaces REKR at position 508–511. EK is an “enterokinase” digestion site with sequence Asp-Asp-Asp-Asp-Lys and is added downstream of NFL. UFO is “uncleaved prefusion-optimized” consists of the sequence Gly-Ser repeated four times replacing residues 548–568. The UNC consists of K510S+R511S. The NT1-5 mutant consists of M535I+L543Q+N553S+Q567K+G588R.

<https://doi.org/10.1371/journal.ppat.1011452.g001>

this question, we generated a panel of mutants, including SOS, NFL, I559P, UFO, A433P, DS, A328G [25] and enterokinase cleavage site (EK) mutants [61], alone and in combination in the JR-FL E168K+N189A gp160ΔCT parent background. These mutants, depicted schematically in Fig 1, were co-expressed with Rev and MuLV Gag plasmids in 293T cells to make VLPs. All amino acid positions are based on HxB2 numbering. MuLV Gag was used because it improves passive gp160ΔCT incorporation onto VLPs compared to HIV-1 or SIV Gag in previous studies [22,62].

A gp120-gp41 linker may grant gp160 with the flexibility for the gp120 and gp41 components to associate in a “near native” conformation. Linkers could therefore be a partial remedy for incomplete gp120/gp41 processing to improve the consistency of Env products. Accordingly, we included NFL linkers [9] in many of our combination mutants. VLP lysates were first compared in reducing SDS-PAGE-Western blots (Fig 2). As expected, NFL eliminated gp120 and gp41 bands (missing red and green dots, respectively in lanes 2–10). Consistent with previous studies [30,34,39,43–46,63,64], we detected two forms of gp160: a “mature” gp160 (gp160m, magenta dots) bearing complex glycans and an “immature” gp160 (gp160i, yellow dots) bearing high mannose glycans. In NFL mutants, the gp120 band of the SOS parent (Fig 2A, lane 1 red dot) was replaced by gp160m (Fig 2A, lane 2, magenta dot), indicating that, in the absence of a NFL linker, gp160m is partially processed into gp120 and gp41. In contrast, gp160i is unaffected by NFL.

I559P increased gp160m mobility so that it almost co-migrated with gp160i (Fig 2, compare lane 2 to lanes 3, 6, 8, 9, 11, 12, 17, and 19). In mutants lacking NFL, I559P impaired gp120/gp41 processing, revealed by the absence of gp120 and gp41 bands (Fig 2A and 2B, compare lane 15 to lanes 17 and 19). I559P also improved Env expression (Fig 2C, compare mutant pairs in lanes 2 and 3, 5 and 6, 7 and 8, 11 and 14, 12 and 13).

Surprisingly, UFO clones expressed very poorly (Fig 2, lanes 4 and 10), perhaps because they were made in context with NFL. Evidently, these two proximal linkers adversely affect folding. Weak bands were only detected when blots were probed with the full gp120 and gp41 MAbs (Fig 2C, lanes 4 and 10). The A433P mutant is intended to disrupt the formation of the bridging sheet required for coreceptor binding, thereby stabilizing the trimer in ground state. Here, A433P slowed Env mobility. This was particularly clear when it was used in combination with I559P that increases Env mobility (Fig 2, compare lanes 3 and 6, 8 and 9, 11 and 12). In the absence of NFL, A433P reduced gp160m, suggesting that it is processed more efficiently (Fig 2, compare lanes 15 and 16). In contrast, DS impaired gp160 processing

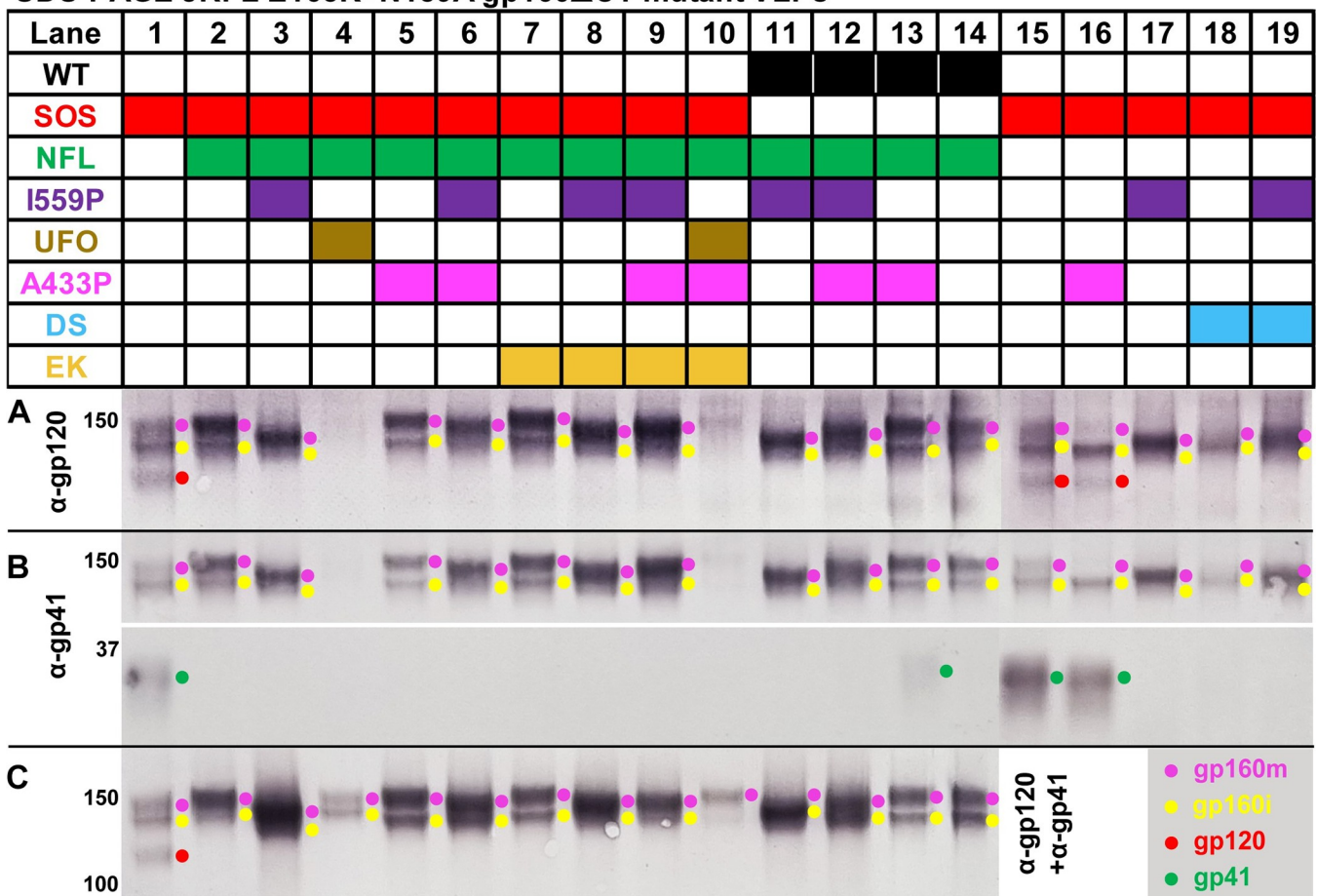
SDS-PAGE JRFL E168K+N189A gp160 Δ CT mutant VLPs


Fig 2. SDS-PAGE-Western blot of gp160 Δ CT mutants. VLPs expressing various JR-FL gp160 Δ CT E168K+N189A mutant combinations were analyzed by reducing SDS-PAGE-Western blot. Duplicate blots were probed with A) anti-gp120, B) anti-gp41 or C) anti-gp120+gp41 MAb cocktails. Env species are indicated by colored dots.

<https://doi.org/10.1371/journal.ppat.1011452.g002>

and reduced expression (Fig 2, compare lanes 15 and 18, 17 and 19). High expression was restored when DS and I559P mutants were used together (Fig 2, lane 19).

The behavior of WT mutants mirrored those of the SOS mutants above (Fig 2, lanes 11–14). WT NFL exhibited gp160m and gp160i bands (Fig 2, compare lanes 2 and 14). I559P and A433P mutants increased or decreased gp160m mobility, respectively (Fig 2, compare lanes 3 and 11, and lanes 5 and 13). I559P and A433P combined led to an intermediate phenotype (Fig 2, compare lanes 3, 5 and 6, 11–13). A faint gp41 band was detected for A433P (Fig 2B, lane 13) suggesting that NFL is slightly sensitive to host proteases in WT mutants, but not in SOS and I559P mutants. Finally, NFL mutants containing an enterokinase site (EK+) were comparable to parental NFL clones (Fig 2A and 2C, compare lanes 2 and 7, 3 and 8, 6 and 9).

Endo H glycosidase reveals high mannose and complex glycan species

Above, we saw that I559P increased gp160m mobility. Possible explanations are i) impaired glycan processing and/or ii) "sequon skipping", reducing the total number of glycans. Without the NFL linker, I559P was also uncleaved, as was DS (Fig 2, lanes 17 and 19). To further investigate, denatured Env from a subset of mutants was digested with endoglycosidase H (endo H)

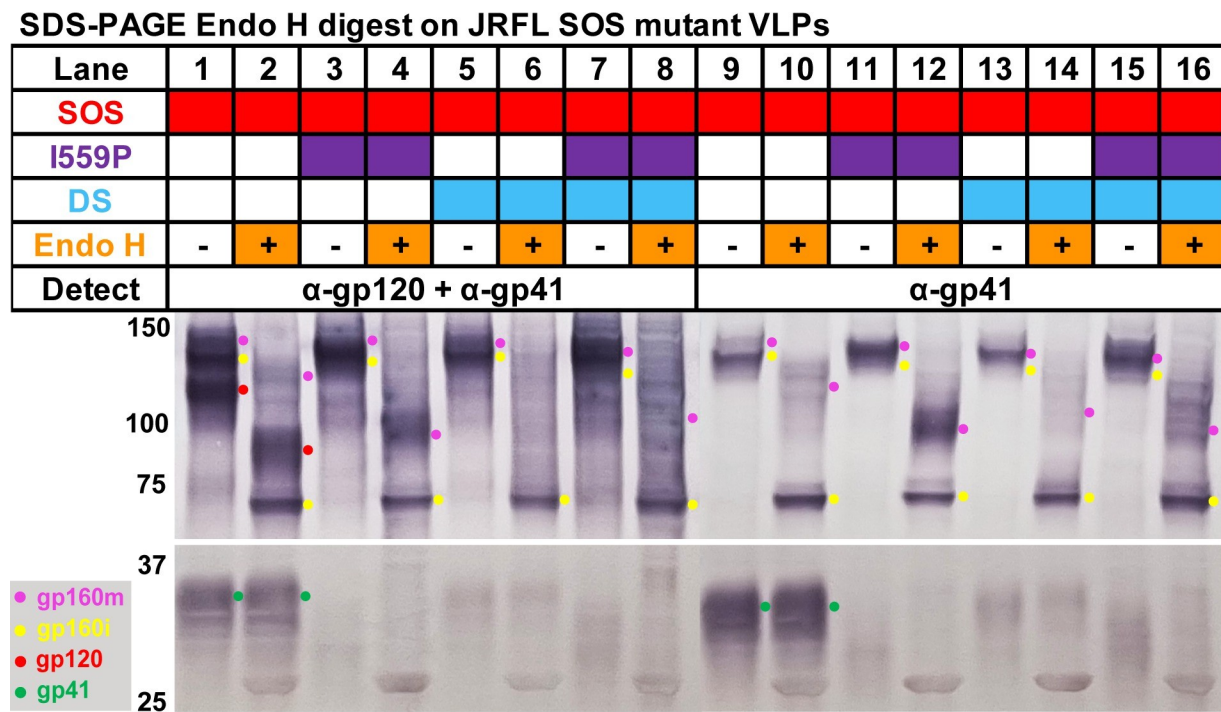


Fig 3. Endoglycosidase H digestion of I559P, DS and I559P+DS gp160 Δ CT mutants. VLPs were lysed and boiled in SDS/DTT, then treated with endo H or PBS. Samples were then analyzed in duplicate SDS-PAGE-Western blots probed with anti-gp120+gp41 MAb cocktail (Lanes 1–8) or anti-gp41 MAb cocktail (Lanes 9–16).

<https://doi.org/10.1371/journal.ppat.1011452.g003>

to selectively remove high mannose glycans, followed by SDS-PAGE-Western blot. Duplicate blots were probed with anti-gp120+gp41 MAb cocktail or anti-gp41 MAb cocktails (Fig 3). SOS "parent" VLP gp120 was partially endo H-sensitive; gp41 was endo H-resistant (Fig 3, lanes 1, 2, 9 and 10, red and green dots). Gp120 and gp41 bands were faint or absent in I559P and DS (Fig 3, lanes 3–8 and 11–16). Instead, I559P gp160m was dominant and, upon endo H treatment, migrated far more rapidly than parent gp160m (Fig 3, lanes 2, 4, 10 and 12, magenta dots). In contrast, endo H-treated DS gp160m was a smear, like parent gp160m, but showing greater endo H sensitivity (Fig 3, lanes 2, 6, 10 and 14). Endo H-treated double mutant gp160m showed an intermediate pattern (Fig 3, compare even numbered lanes). All samples showed discrete, fully endo H-sensitive high mannose gp160i (Fig 3, yellow dots). Overall, this confirms that I559P and DS mutants cause folding defects that result in poor gp160 processing. Furthermore, I559P increases gp160m's endo H sensitivity, suggesting a greater prevalence of high mannose glycans.

Enterokinase (EK) digestion generates gp120/gp41

An NFL linker-embedded enterokinase cleavage site (EK+) may provide a way to cleave gp120/gp41 post-expression [61]. We compared the EK sensitivity of NFL mutants with or without I559P and EK sites, i.e., samples from Fig 2, lanes 2, 3, 7 and 8. EK digestion of EK+ but not EK- clones led to the appearance of gp120 and gp41 bands (Fig 4A and 4B, compare lanes 11 and 15 to lanes 3 and 7; red and green dots, respectively). Concomitantly, gp160m was depleted (Fig 4A and 4B, compare magenta dots in lanes 9, 11, 13 and 15). I559P did not appear to affect gp160m depletion by EK digestion, (Fig 4B, compare magenta dots in lanes 10 and 12, 14 and 16).

SDS-PAGE Enterokinase & Endo H digest on intact SOS NFL mutant VLPs

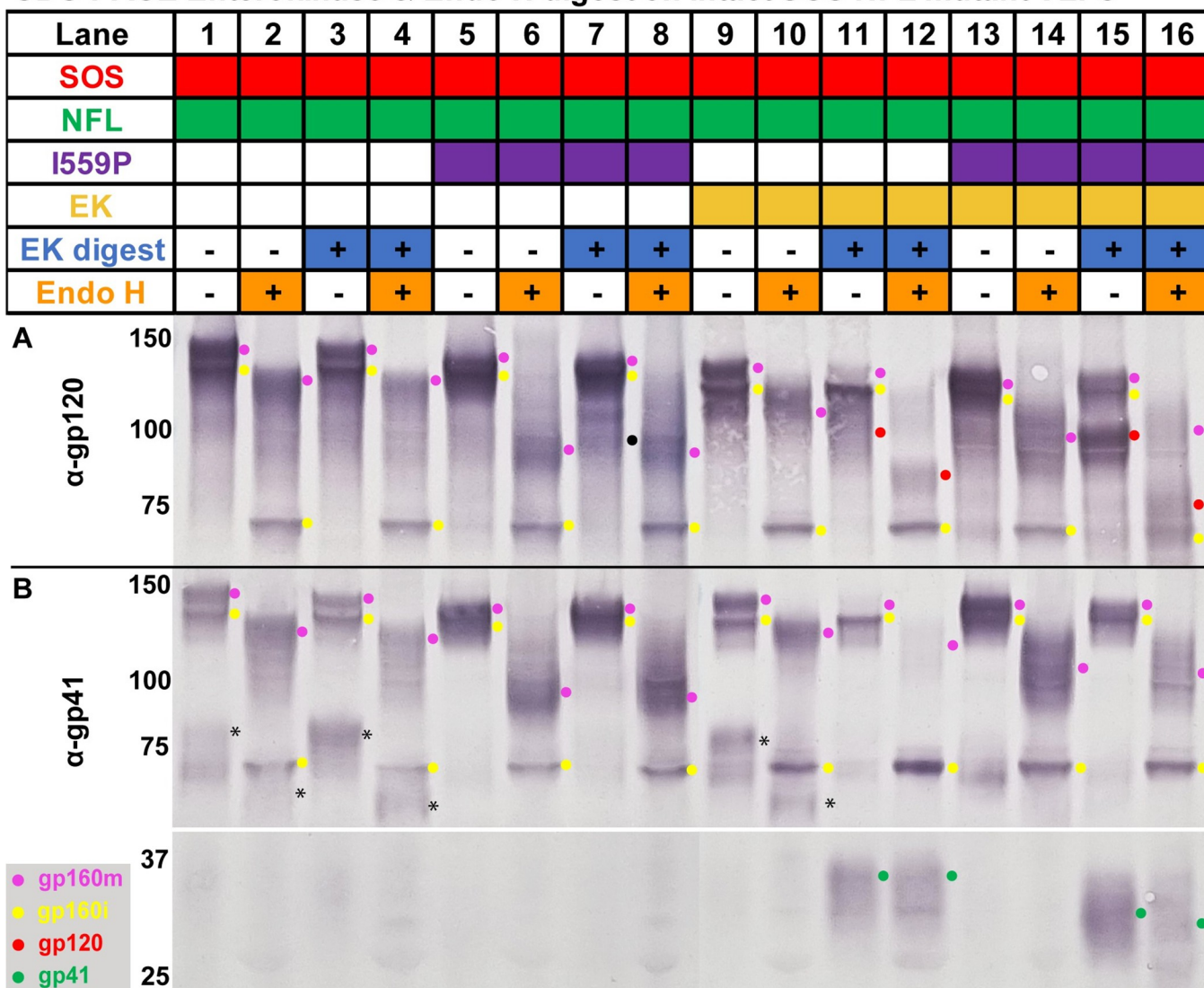


Fig 4. Enterokinase processing and endoglycosidase H digestion of gp160 Δ CT SOS NFL mutants into gp120/gp41. VLPs were digested with enterokinase or PBS for 30h at 37°C, then lysed, incubated with endo H or PBS then analyzed in reducing SDS-PAGE-Western blot and probed with A) anti-gp120 or B) anti-gp41 MAb cocktails. The asterisk (*) marks an ~80kDa band detected by anti-gp41 MAb cocktail in parent (non-I559P) samples, that suggests non-specific digestion, perhaps of the V3 loop, even in the absence of EK enzyme. The black dot detected in the anti-gp120 MAb cocktail (Lane 7) represents the non-specific digestion of gp160m by the EK enzyme.

<https://doi.org/10.1371/journal.ppat.1011452.g004>

As in Fig 3, I559P gp160m bands migrated faster with endo H (Fig 4A and 4B, compare even numbered lanes). EK-digested I559P gp120 and gp41 bands both migrated faster than their parental equivalents (Fig 4A and 4B, compare lane 16 to lane 12). Indeed, I559P gp41 was partially endo H-sensitive, unlike the parent, suggesting modified glycan maturation (Fig 4B, compare gp41 green dots in lanes 15 and 16 to lanes 11 and 12). We infer that I559P reduces glycan maturation in *both* gp120 and gp41.

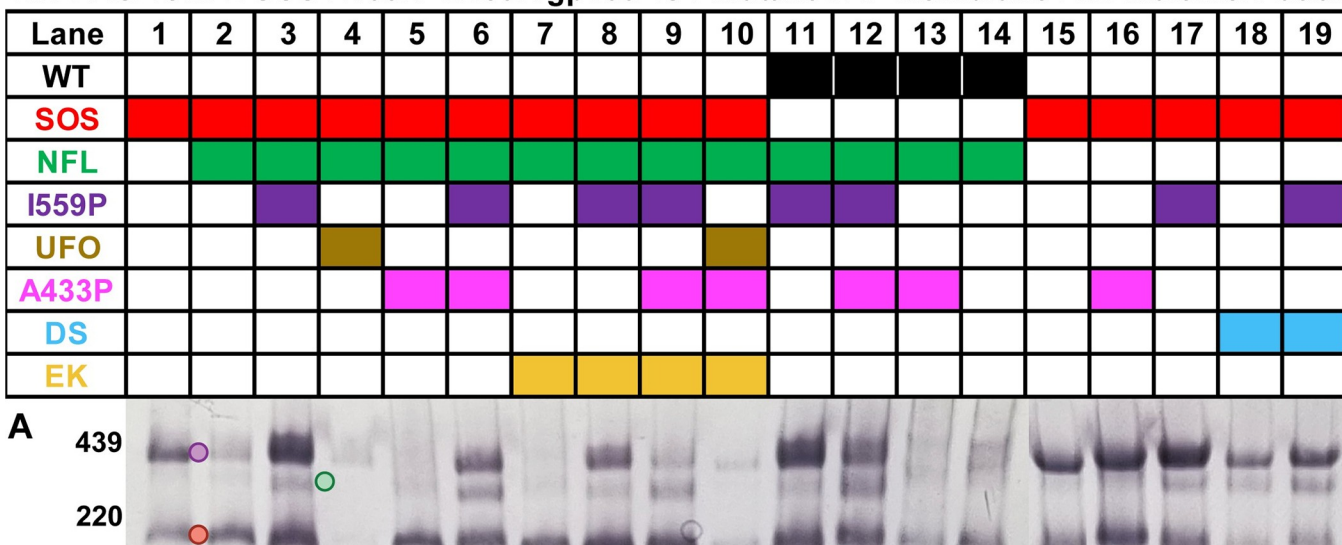
Despite lacking an EK site, I559P EK- gp160m was partially digested non-specifically such that a weak band corresponding to gp120 was detected (Fig 4A, lane 7, black dot). Although gp41 was absent, an ~80kDa band was detected by anti-gp41 MAb cocktail in parent (non-I559P) clones (Fig 4B, black asterisks in lanes 1, 3 and 9). This also suggests non-specific

digestion, perhaps of the V3 loop, even in mock incubations (i.e., no EK added). These bands were diffuse and only partially endo H-sensitive, suggesting that they derive from gp160m (Fig 4B, black asterisks in lanes 2, 4 and 10). In stark contrast, gp160i was insensitive to EK digestion (Fig 4A and 4B, yellow dots), suggesting that the EK site is sequestered. Overall, EK cleaves gp160m, but does not cleave gp160i.

BN-PAGE reveals various forms VLP Env and their lateral stability

As we reported previously, SOS gp160 Δ CT resolves as trimers and monomers in BN-PAGE [22,30] (Fig 5A, lane 1). The trimer band includes functional, cleaved gp120/gp41, while the monomer comprises of gp160m and gp160i. SOS NFL also exhibited trimers and monomers. However, trimer band density was weaker (~35%), and the monomer band density was stronger (~160%) relative to SOS (Fig 5A, compare lane 1 and 2; S1A and S1C Fig). This suggests

BN-PAGE JRFL SOS E168K+N189A gp160 Δ CT mutant VLP-Membrane Env multimerization



BN-PAGE Enterokinase digests on JRFL SOS NFL mutant VLPs

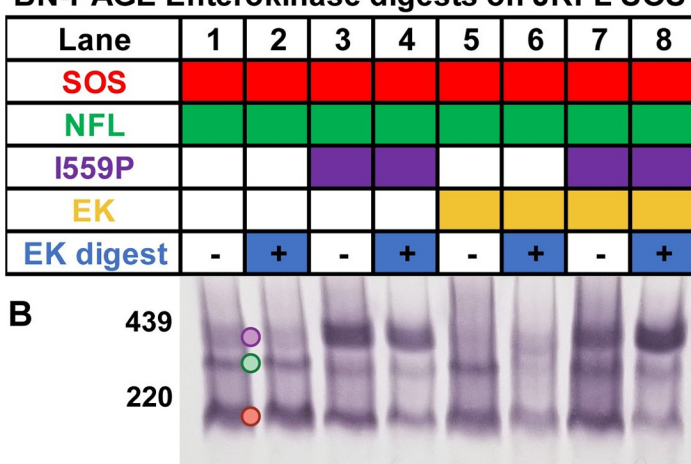


Fig 5. BN-PAGE-Western blot of gp160 Δ CT mutants. A) The same mutants in Fig 2 were analyzed by BN-PAGE-Western blot, detecting with anti-gp120 +gp41 MAb cocktail. Densitometry analysis of trimer, dimer and monomer band is shown in S1 Fig) BN-PAGE analysis of enterokinase-treated samples from Fig 4. Env species are indicated by colored dots.

<https://doi.org/10.1371/journal.ppat.1011452.g005>

that gp160 either fails to form trimers effectively, or that they are unstable upon detergent lysis and electrophoresis. In other words, gp120/gp41 cleavage promotes lateral trimer stability [29,33,65]. Overlaying the I559P mutation increased both trimer and monomer staining (Figs 5A, compare lanes 1–3, and S1). A putative dimer was also present in all I559P and DS mutants (Figs 5A, lanes 3, 6, 8, 9, 11, 12, 17, 18, and 19, and S1B). UFO mutants expressed poorly, consistent with the SDS-PAGE blot analysis above (Figs 2 and 5A, lanes 4 and 10). NFL A433P Env resembled the NFL parent, although the weak trimer band was more diffuse (Fig 5A, compare lanes 2 and 5). When A433P was combined with I559P, a weak and fast-moving trimer was restored (Fig 5A, compare lanes 3 and 6). EK+ versions of these mutants exhibited band patterns like their EK- equivalents, but expression was weaker (Fig 5A, compare lanes 2 and 7, 3 and 8, 6 and 9).

WT NFL I559P expressed well, with dimers like its SOS equivalent (Figs 5A, lanes 3 and 11, and S1). Overlaying A433P reduced Env expression, like its SOS counterpart (Fig 5A, compare lanes 3 and 11 to lanes 6 and 12). WT NFL A433P expressed poorly and was diffuse, again like its SOS analog (Fig 5A, lanes 5 and 13). WT NFL also expressed weakly, with diffuse bands (Fig 5, lanes 2 and 14).

We next evaluated SOS clones without NFL. SOS A433P exhibited trimers and monomers, like the SOS parent (Fig 5A, lanes 15–16), although monomer and trimer mobility were reduced. I559P exhibited predominant trimer, modest monomer and a faint dimer (Fig 5, lane 17). DS exhibited weak trimer and monomer and a faint dimer (Fig 5, lane 18). Combining DS and I559P resulted in an intermediate phenotype (Fig 5A, compare lanes 17–19). Overall, we infer that I559P improves expression and that lateral trimer stability is attained either by gp120/gp41 cleavage or by I559P.

Enterokinase (EK)-mediated gp120/gp41 processing increases lateral trimer stability

Since gp120/gp41 cleavage increases lateral stability, we investigated if post-expression EK-mediated cleavage of EK+ NFL gp160 Δ CT into gp120/gp41 affects the trimer in BN-PAGE. We treated clones in Fig 5A lanes 2, 3, 7 and 8 with or without EK enzyme (Fig 5B). Mock treatment led to the appearance of dimers in non-I559P samples (Fig 5B, lanes 1 and 5) that were absent in the corresponding untreated samples (Fig 5A, lanes 2 and 7). EK digestion of EK+ clones led to changes in band patterns; I559P showed more trimer and less monomer (Fig 5B, lanes 7–8). EK digestion of the non-I559P EK+ clone led to weaker monomer and dimer (Fig 5B, lanes 5 and 6). In contrast, digestion of EK- samples had little or no effect (Fig 5B, lanes 1–4).

NT1-5, UNC, A328G+/-D197N effects on membrane trimer

The NT1-5 combination mutant (M535I+L543Q+N553S+Q567K+G588R), which affects the “b” positions of the highly conserved gp41 N helix, was reported to reduce gp160 monomer expression without affecting trimer expression [17,20]. Here, we evaluated the effects of NT1-5 in the context of JR-FL SOS gp160 Δ CT. To enable us to better judge the effects of NFL, we also made a double mutant (K510S+R511S) [66] to create a simple uncleaved (UNC) mutant.

In SDS-PAGE, NT1-5 Env showed slightly reduced gp120/gp41 processing (S2A Fig, lanes 1, 2, 4 and 5). As expected, UNC lacked gp120 and gp41, and showed a strong gp160m band (S2A Fig, lanes 3 and 6). In BN-PAGE, NT1-5 increased trimer and decreased monomer (S2B Fig, compare lanes 1 and 2). In contrast, UNC was predominantly monomer, with weak dimer and trimer (S2B Fig, lane 3). This latter pattern resembles NFL (Fig 5A, lane 2), except that the

dimer is more prominent for UNC. Overall, this data suggests that, like I559P, NT1-5 laterally stabilizes UNC trimers and modestly reduces gp120-gp41 processing.

Previously, we used the “globally sensitive” A328G mutant to measure non-neutralizing antibodies in vaccine sera [26]. A328G was sensitive to non-NAbs 39F and 15e (S2C Fig, left panels, open symbols). Interestingly, glycan hole filling mutant D197N was somewhat b12-resistant compared to the parent but became highly b12-sensitive when combined with A328G mutation. This overt change was mirrored by higher sensitivity to 39F and 15e compared to the other A328G mutant. In addition, PG16 sensitivity was lost, consistent with a “globally sensitive” conformation. In BN-PAGE, A328G showed reduced trimer, suggesting reduced lateral stability (S2D Fig, bottom panel, lanes 2 and 4). In SDS-PAGE blots, all clones showed similar patterns (S2D Fig, top panel). We therefore chose SOS E168K+N189A+D197N+A328G as a prototype globally sensitive mutant for further experiments.

BS³ crosslinking effect on membrane trimer

Although SOS trimers are stabilized in the apical plane by a disulfide bond, they may dissociate laterally following lysis and BN-PAGE [30]. To check this point, we used BS³ to crosslink selected clones before VLP lysis. Crosslinking significantly reduced monomer in all cases, particularly for I559P or DS (Fig 6, compare lanes 6, 8, 10, 12 to lanes 5, 7, 9, 11). Notably, SOS NFL I559P behaved similarly to SOS I559P (Fig 6, lanes 5, 6, 9 and 10). Since I559P prevents gp120/gp41 cleavage, these clones differ only by the length of the peptide linking gp120 and gp41, which evidently has little effect here. For non-I559P mutants, some monomer shifted upwards slightly with BS³ (Fig 6, lanes 2 and 4, black asterisks). The survival of some trimer in the face of boiling in SDS and DTT verifies that BS³ crosslinking was effective (Fig 6, lanes 13 and 14). Overall, this is consistent with the idea that Env is mostly if not all trimeric but different forms exhibit varying lateral stability.

BN-PAGE BS³ crosslinking effect on pre-VLP lysis

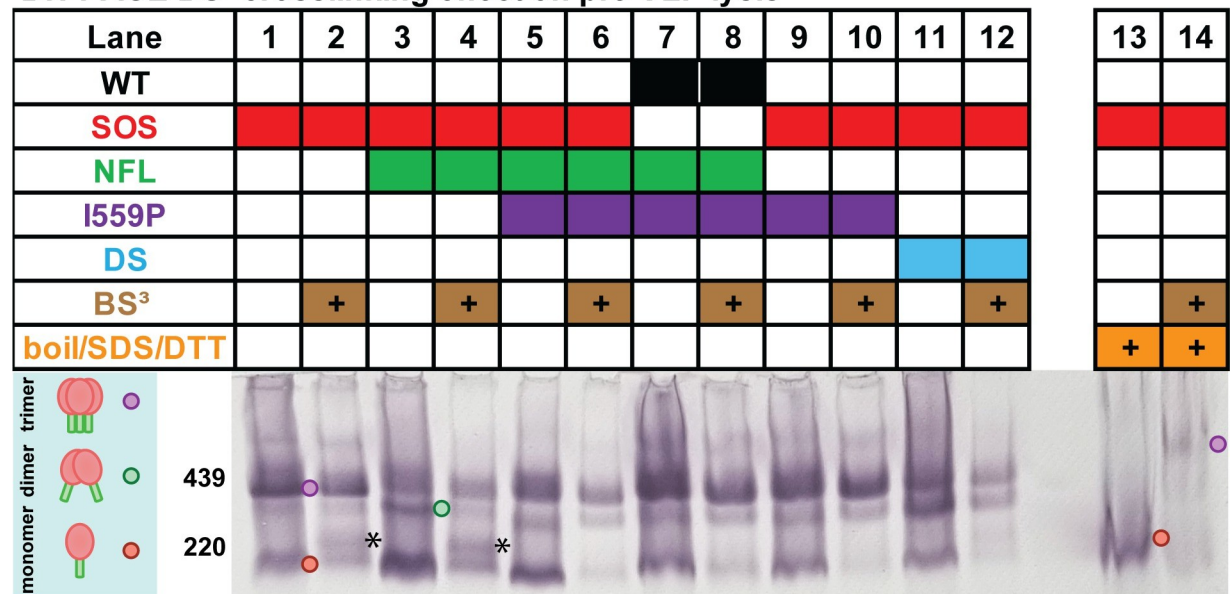


Fig 6. Effect of lysis on gp160ΔCT trimer stability in the presence of BS³ crosslinker. VLPs corresponding to lanes 1, 2, 3, 11, 17 and 18 of Figs 2 and 5 were crosslinked with and without BS³, then analyzed by BN-PAGE-Western blot, detecting with anti-gp120+gp41 MAb cocktail. Crosslinking efficiency was checked by boiling crosslinked or PBS-treated SOS VLPs in SDS and DTT (lanes 13 and 14). The asterisk (*) marks monomer shifted upwards with BS³ crosslinking. Env species are indicated by colored dots.

<https://doi.org/10.1371/journal.ppat.1011452.g006>

Effect of DS on membrane trimer-sCD4 sensitivity

The DS mutant was designed based on the SOSIP gp140 trimer structure to insert a disulfide between positions 201 and 433 to restrict soluble CD4 (sCD4) binding and downstream conformational changes [11]. Soluble DS gp140 trimers bind only one molecule of sCD4, preventing full exposure of CD4-inducible (CD4i) and V3 epitopes. To check this with membrane trimers, excess 4 domain sCD4 was incubated with parent or DS VLPs, followed by a wash and BN-PAGE to evaluate shifts. DS trimers were shifted like the parent trimers, suggesting the binding of 3 sCD4 molecules ([S3 Fig](#), compare lanes 2 and 4) [30]. Overall, the similar sCD4 binding patterns suggest that DS does not limit sCD4 binding to membrane trimers.

Probing VLP antigenicity by native PAGE shifts

Authentic, functional trimers are likely to be important for vaccine efficacy. A key question is whether trimer stabilizing mutations have unwanted antigenic consequences. Flow cytometry and cell ELISA have been used to appraise binding of NAbS and non-NAbS [10,29]. However, these methods can not differentiate between binding to native trimers or other forms of Env presented on cell surfaces, including gp160m. “BN-PAGE shifts” [30] can provide some clarity on this point by revealing MAb complexes with different Env isoforms. We first compared MAb binding to SOS and SOS NFL I559P trimers ([Fig 7](#)) using a panel of NAbS directed to CD4bs, V2 and interface epitopes. Non-NAbS directed to the V3 and CD4bs were included to monitor unwanted epitope exposure. To detect MAb-Env complexes, blots were initially probed directly with anti-human IgG AP conjugate ([Fig 7B and 7D](#)). Conversely, the blots in [Fig 7A and 7C](#) were probed with anti-Env cocktails to detect *all* forms of Env, regardless of whether it is complexed with MAb.

CD4bs MAbs

VRC03 and b12 depleted uncomplexed SOS or SOS NFL I559P trimers ([Fig 7A and 7C](#), compare lanes 1, 2 and 3). In contrast, 15e did not bind to either trimer ([Fig 7A and 7B](#), lane 4). ~220kDa bands were observed with b12 and 15e ([Fig 7A and 7C](#), lanes 3 and 4 asterisks). There were no bands in lanes 3 and 4 of [Fig 7B and 7D](#) that could account for the ~220kDa bands in the corresponding lanes [Fig 7A and 7C](#) (see asterisks in lanes 3 and 4), suggesting that these are ‘Env only’ bands, not MAb-Env complexes. Notably, the monomer was only partially depleted at best by MAb binding.

V3 MAb

39F, 447-52D and CO11 did not deplete either trimer ([Fig 7A and 7C](#), compare lane 1 to lanes 5–7). 39F and 447-52D induced bands at ~440kDa. The same bands were present in the corresponding “conjugate alone” blots ([Fig 7A–7D](#), lanes 5–6), suggesting that they are MAb-Env complexes. In contrast, CO11 induced a ~300kDa band ([Fig 7A and 7C](#), lane 7). To try to understand the ~440kDa complexes induced by 39F and 447-52D, we evaluated 39F shifts of the SOS NFL ([Fig 8A](#), lane 2). Although SOS NFL resolves mostly as a monomer in BN-PAGE, 39F still induced a ~440kDa species, indicating that 39F binds to uncleaved trimers and prevents them from dissociating laterally upon lysis ([Fig 8A](#), lane 1).

V2 MAb

PGT145, PG16, CH01, VRC38 and PC64 35K all bound to both SOS and SOS NFL I559P ([Fig 7A and 7C](#), lanes 8–12), albeit with differences. SOS trimers were completely depleted by PGT145 and PG16 ([Fig 7A and 7C](#), lanes 8–9). PGT145, PG16, CH01 and PC64 35K shifts of SOS resulted in two high molecular weight bands at ~440kDa and ~480kDa ([Fig 7A](#), lanes 8, 9,

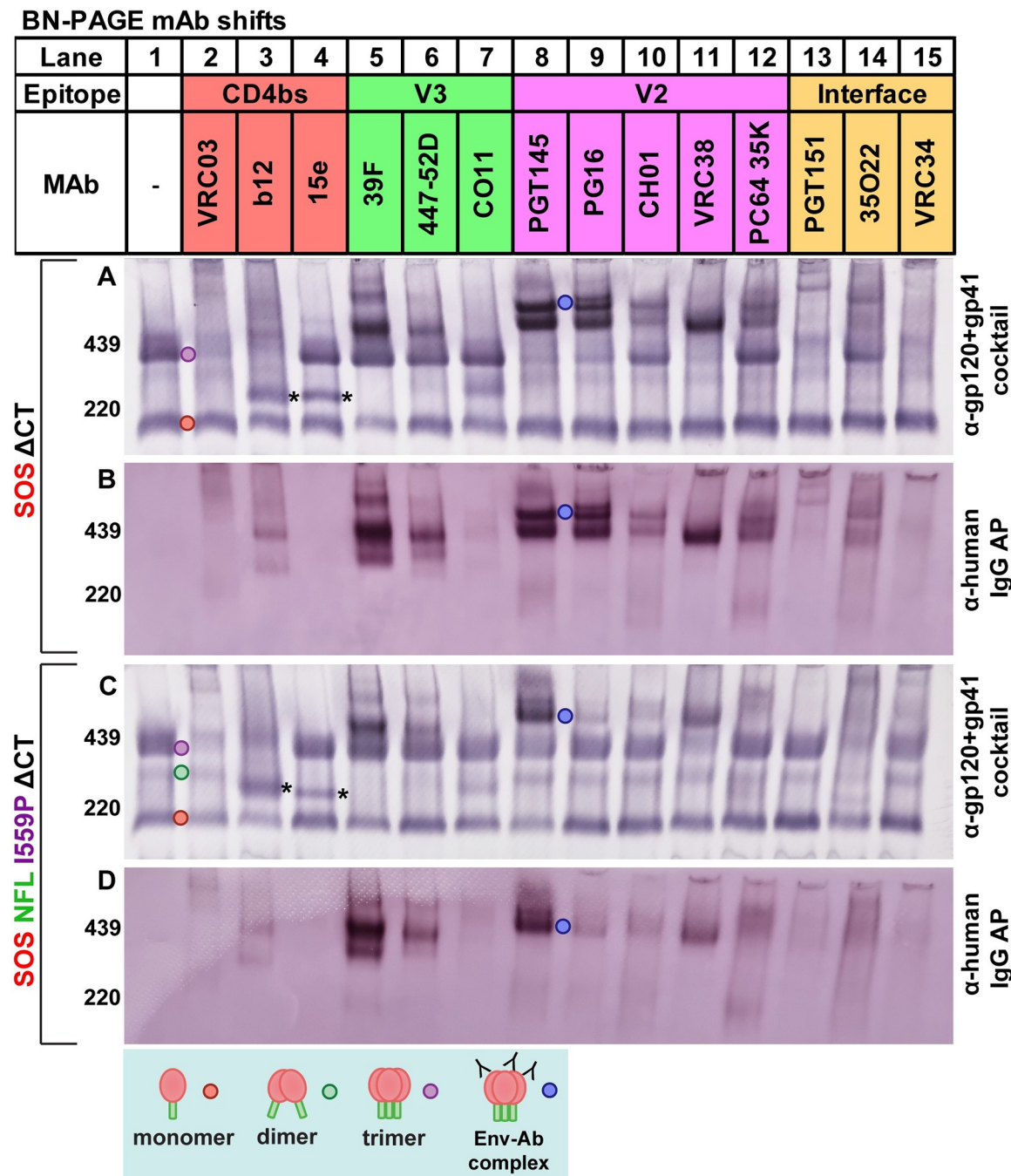


Fig 7. MAb binding to JR-FL gp160 Δ CT E168K+N189A in BN-PAGE “shifts”. MAbs were mixed with SOS VLP (A and B) or SOS NFL I559P VLP (C and D) and were incubated at 37°C for 1h, then washed, lysed and analyzed by BN-PAGE-Western blot, probing with anti-gp120+gp41 MAb cocktail, followed by anti-human IgG AP conjugate (A and C) or just the anti-human IgG AP conjugate (B and D). The asterisk (*) marks a ~220kDa observed with b12 and 15e, possibility arise from decreased lateral stability during MAb binding.

<https://doi.org/10.1371/journal.ppat.1011452.g007>

10 and 12). However, for SOS NFL I559P, only a ~440kDa band was clear with PGT145 (Fig 7C, lane 8). VRC38 also shifted SOS more completely than SOS NFL I559P (Fig 7A and 7C, lane 11). Indeed, V2 NAb binding to SOS NFL I559P was generally weak: trimer depletion was marginal and shifted bands were fainter (Fig 7C, lanes 8–12). The same blots probed with only

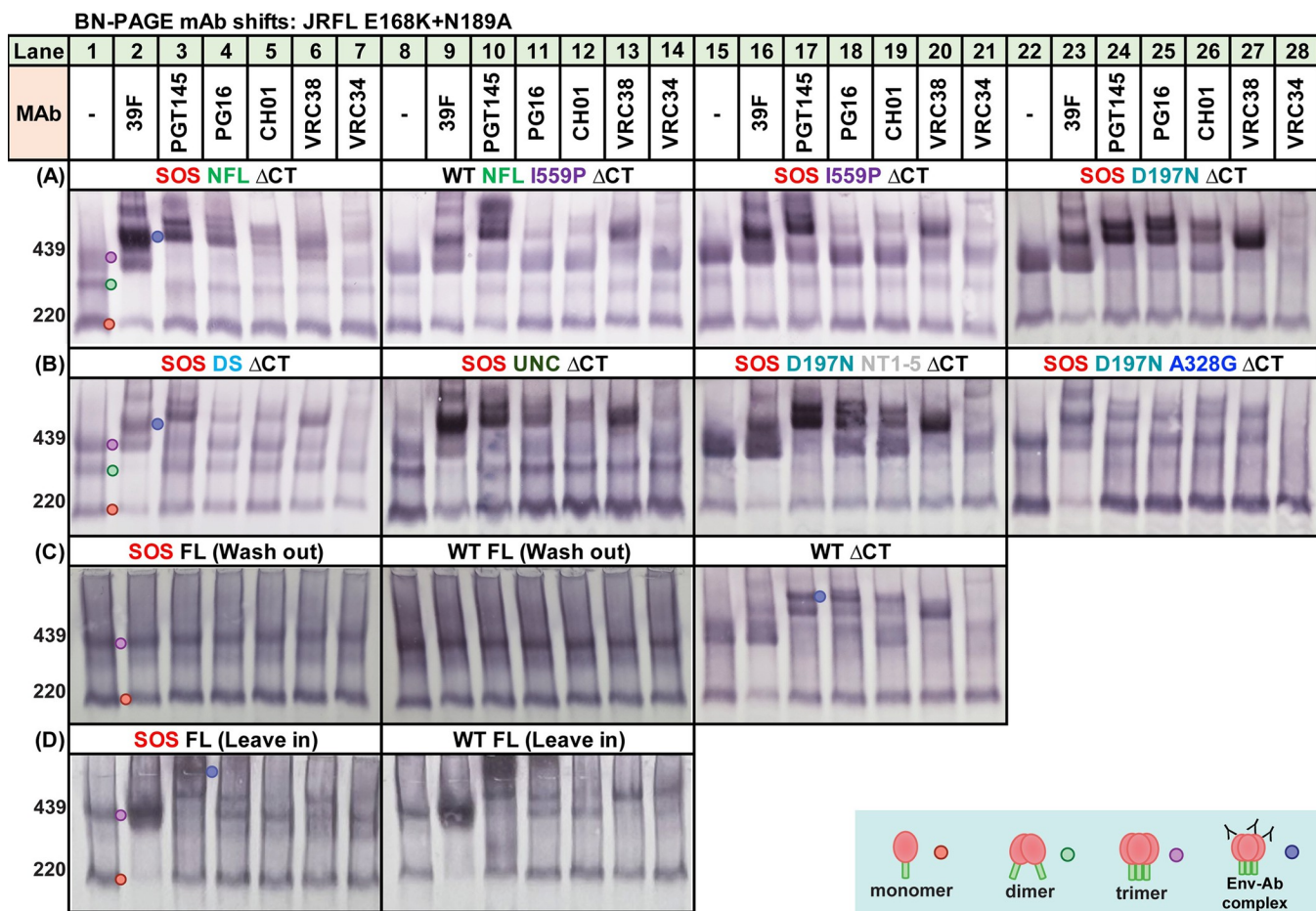


Fig 8. Dissecting mutant contributions to antigenic profiles by BN-PAGE mAb “shifts”. MAb shifts were performed with various mutants and resolved on BN-PAGE, detecting with anti-gp120+gp41 MAb cocktail. Mutants are all JR-FL gp160ΔCT E168K+N189A, except for some full length (FL) gp160 clones. (A) SOS NFL (lanes 1–7), WT NFL I559P (lanes 8–14), SOS I559P (lanes 15–21), SOS D197N (lanes 22–28); (B) SOS DS (lanes 1–7), SOS UNC (Lanes 8–14), SOS D197N NT1-5 (lanes 15–21), SOS D197N+A328G (lanes 22–28); (C) SOS FL-Wash out (lanes 1–7), WT FL-Wash out (lanes 8–14), WT (lanes 15–21); (D) SOS FL-Leave in (lanes 1–7), WT FL-Leave in (lane 8–14). For VLPs bearing FL Env, excess MAbs are either removed by washing in PBS (Wash out) or not removed (Leave in). UNC mutant is gp160ΔCT SOS E168K+K510S+R511S.

<https://doi.org/10.1371/journal.ppat.1011452.g008>

anti-IgG AP conjugate (Fig 7B and 7D, lanes 8–12) lend further support the weaker V2 NAb binding to SOS NFL I559P, contrasting sharply with the equivalent binding of 39F and 447-52D to uncleaved Envs of the two mutants (Fig 7B and 7D, lanes 5 and 6).

To better understand PGT145 binding patterns, we examined intermediate mutants. The 440kDa and 480kDa doublet observed in Fig 7A, lane 8 was prominent only in clones that permit at least some gp120/gp41 processing such as SOS D197N (Fig 8A, lane 24), SOS D197N NT1-5 (Fig 8B, lane 17) and WT ΔCT (Fig 8C, lane 17). However, in those with poor or no processing (e.g., SOS NFL, WT NFL I559P, SOS I559P, SOS DS, SOS UNC), the 480kDa band was weak or absent. This suggests that PGT145 binding creates distinct complexes with cleaved gp120/gp41 trimers (480kDa band) and UNC trimers (440kDa band).

Interface NAb

PGT151 and VRC34 depleted SOS trimers but not SOS NFL I559P trimers, consistent with the importance of gp120/gp41 processing for binding (Fig 7A and 7C, lanes 13 and 15). In

contrast, 35O22 depleted SOS NFL I559P trimers more effectively than SOS trimers ([Fig 7A and 7C](#), lane 14). Since 35O22 binding is subject to glycan clashes [46], the improved binding may reflect glycan changes associated with I559P. We revisit this point below.

Other NAbS

Lastly, we further evaluated the two main mutants of [Fig 7](#) in BN-PAGE shifts with a broader panel of MAbs ([S7 Fig](#)). As expected, 2G12, PGT121, 2F5 and 4E10 exhibited comparable binding patterns with both mutants. Neither 7B2 nor CR3022 bound. In the case of 7B2, the SOS mutation occludes the gp41 cluster I epitope, while lack of CR3022 binding confirms specificity.

Intermediate mutants reveal the dominant effect of I559P on Env antigenic profile

We further investigated antigenic differences using a focused MAb panel with intermediate mutants. SOS NFL was more V2-sensitive than SOS NFL I559P (compare [Fig 7C](#) to [Fig 8A](#), lanes 3–6), further emphasizing the adverse effect of I559P on V2 epitopes. Accordingly, WT NFL I559P ([Fig 8A](#), lanes 10–13) and SOS I559P ([Fig 8A](#), lanes 17–20) showed only modest V2 NAb binding. Overall, V2 NAb binding to I559P-bearing mutants was weak, particularly for PG16 and CH01. Neither SOS nor NFL contributed to this effect. Binding of V2 MAbs to SOS DS and D197N NT1-5 was also weak: like I559P mutants, PG16 and CH01 were markedly affected ([Fig 8B](#), lanes 4, 5, 18 and 19). In contrast, like the SOS parent, SOS D197N ([Fig 8A](#), lanes 25 and 26) showed robust V2 NAb binding; PG16 and CH01 depleted the uncomplexed trimer effectively. VRC34 binding to I559P mutants was also weak ([Fig 8A](#), lanes 14 and 21). In contrast, 39F binding to all mutants was comparable, except for full-length (FL) clones in the wash out method (covered below). Notably, SOS I559P ([Fig 8A](#), lanes 15–21) is a close relative of SOS NFL I559P ([Fig 7C](#)), both being uncleaved and differing only in terms of the linker (UNC vs NFL). This difference did not register in BN-PAGE shifts: V2 NAb binding was poor in both cases. WT ΔCT exhibited a very similar pattern to SOS ΔCT (compare [Fig 7A](#) to [Fig 8C](#), lanes 15–21), suggesting that SOS exerts only mild antigenic effects. Globally sensitive SOS D197N+A328G exhibited weak V2 NAb binding ([Fig 8B](#), lanes 24–27), consistent with the expected loss of these epitopes.

Analysis of full-length gp160 VLPs

Much of our prior vaccine development work has used gp41 truncated Env (ΔCT), due its improved expression, gp120/gp41 processing and minor effects on antigenic profile [22]. However, in some Env strains, SOS and ΔCT mutations can affect antigenic profile [36,38,67,68]. We therefore evaluated WT and SOS JR-FL clones in ΔCT and gp160 full-length (FL) formats in SDS-PAGE with or without endo H, then probed in duplicate blots with gp120 and gp41 MAb cocktails. FL clones exhibited very poor gp120/gp41 processing, revealed by faint endo H-resistant gp41 bands ([S4A Fig](#), lanes 9–16). Corresponding gp120 bands were also weak ([S4A Fig](#), compare lanes 3, 4, 7 and 8 to 1, 2, 5 and 6). As expected, gp160 and gp41 bands in FL clones migrated slower due to additional gp41 mass. Notably, FL clones exhibited very strong endo H-sensitive gp160i bands ([S4A Fig](#), compare yellow dots in lanes 3 and 7 with 1 and 5), suggesting an elevated rate of misfolding.

In our standard BN-PAGE shift protocol, MAb-VLP complexes are washed to remove unbound MAb prior to lysis and electrophoresis. Intriguingly, in this format, both FL clones *did not show binding by any MAb* ([Fig 8C](#), lanes 1–14). However, binding was observed *when the wash step was omitted*. 39F robustly shifted WT and SOS FL monomers ([Fig 8D](#), lanes 2

and 9). FL shift patterns ([Fig 8D](#), lanes 1–14) resembled ΔCT counterparts (Figs [7A](#) and [8C](#) lanes 15–21). However, VRC38 and VRC34 binding to WT FL trimer appeared to be stronger than to SOS FL trimer ([Fig 8D](#), compare lanes 6–7 and lanes 13–14) or SOS ΔCT mutant ([Fig 7A](#), lanes 11 and 15). Furthermore, CH01 showed little or no binding on FL clones and PG16 was only partially saturating. It should be noted that these differences may be driven by the significantly elevated representation of the gp160i isoform in FL clones, which may differ in antigenic properties compared to gp160m and native trimers.

Two possibilities may account for the lack of MAb binding to FL in the washout format. First, that FL undergoes a conformational change upon VLP lysis that results in MAb dissociation, or second that none of these MAbs in fact bind to FL trimers on VLP surfaces. Instead, MAb binding in the “leave in” format occurs only *after* VLP lysis. To dissect these possibilities, we checked PGT145 in further BN-PAGE shifts in which BS³ was used to cross-link any PGT145-trimer complexes to prevent MAb dissociating upon lysis ([S5 Fig](#)). In addition to comparing the effects of washing after PGT145 incubations, we also compared the effects of washes after BS³ crosslinking. We found that PGT145 failed to shift trimer in any format that included a wash, even when BS³ was added ([S5 Fig](#), compare lanes 7 and 12). In the “leave in” format, there was an additional low molecular weight band when BS³ was added, without subsequent washing ([S5 Fig](#), lane 8). This band was not observed when PGT145 was omitted ([S5 Fig](#), lane 6), so this could be free MAb that pellets with VLP due to non-specific cross-linking but is not bound to Env. Taken together, this data supports that the second possibility, that MAbs simply do not bind to FL on intact VLPs. Instead, they only bind *after* lysis.

We next explored the effects of SOS and ΔCT mutations in another strain, PC64 MRCA from a subtype A-infected donor [69]. SDS-PAGE blots revealed smearable gp160 and gp120 bands in ΔCT format but tighter bands in FL format, suggesting more uniform glycans ([S4B Fig](#), compare lanes 1–4). Like JR-FL ΔCT, PC64 ΔCT exhibited far more efficient gp120/gp41 processing than its FL counterpart. In BN-PAGE, SOS appeared to improve trimer and monomer expression relative to WT (regardless of ΔCT or FL), and ΔCT clones were better expressed ([S4C Fig](#)). Gp120 shedding was detected for WT ΔCT, resulting in gp41 stumps ([S4C Fig](#), compare lanes 3 to lane 1).

The neutralization sensitivity profiles of PC64 MRCA WT ΔCT and FL clones were similar ([S6 Fig](#)). SOS FL was insufficiently infectious and was therefore omitted from this analysis. 14E sensitivity was modestly increased by SOS in ΔCT format, as was b12 sensitivity. Correspondingly, PG16 sensitivity was reduced. All clones were CH01-resistant. Collectively, this data suggests that FL clones exhibit weaker gp120/gp41 processing and expression. Furthermore, in contrast to the mild effect of SOS in the JR-FL strain, SOS in the context of the PC64 trimer results in a shift towards a “globally sensitive” phenotype. Therefore, the effects of some mutations are universal (expression and cleavage), but others (NAb sensitivity) are context dependent.

Probing VLP antigenicity by virus capture

To further probe the antigenic effects of modifications, we tested the ability of immobilized MAbs to capture VLPs. SOS VLPs were effectively captured by 2G12, PGT145, PG16 and VRC38. CH01 and PC64 35K were less effective among the V2 mAbs. 39F and 447-52D efficiently captured SOS VLPs, while CO11 capture was poor ([S8A Fig](#)). This is consistent with BN-PAGE shifts, where 39F and 447-52D bound more effectively ([Fig 7B](#)). On the other hand, these V3 MAbs neither bound native trimer ([Fig 7A](#)), nor neutralized ([S8B Fig](#)). PGT121, VRC01, VRC03, b12 and 15e all captured effectively ([S8A Fig](#)). PGT151, 35O22 and VRC34 captured moderately. 10e8, but not 2F5, captured well. 7B2 and 2.2B both captured poorly, as

SOS eliminates these epitopes [30]. Overall, most NAbs captured with at least modest efficiency. Non-NAbs (39F, CO11, 15e) variably captured, presumably via binding gp160m.

Previously, we found that JR-FL WT and SOS PVs exhibited similar neutralization profiles, as did ΔCT [60]. However, this comparison did not include the ‘new wave’ of bNAbs reported since 2009. We therefore compared NAb sensitivity profiles of WT, SOS, FL and ΔCT using a comprehensive set of MAbs (S8B Fig). SOS FL infectivity was weak, (S9 Fig), and was therefore excluded. The 3 other clones exhibited largely consistent profiles (S8B Fig). However, SOS gp160ΔCT was more sensitive to 2G12, b12, 10E8 and 2F5 compared to WT gp160ΔCT. The additional sensitivity to MPER MAbs is afforded by the disulfide bond that must be broken by exposure to reducing agent, providing more time for these MAbs to neutralize.

Since the 2G12 epitope is constitutively exposed [10,37,40], relative 2G12 capture can be used to standardize capture for each Env clone, regardless of any expression differences. There was a ~2-fold range of 2G12 capture efficiency, with SOS NFL A433P being most sensitively captured, while both WT and SOS FL were the least well captured (S10A Fig).

We next evaluated JR-FL mutant MAb capture, expressed as % relative to 2G12 (Fig 9). Capture of each VLP clone was compared to SOS-VLPs, testing for significant differences by Kruskal-Wallis non-parametric rank test. Capture of WT ΔCT and SOS ΔCT was similar. Modest differences in PGT145, PG16 and CH01 capture were not significant. Conversely, VRC38 capture of WT FL was significantly weaker. 15e and 39F capture of FL clones was weaker than their ΔCT counterparts.

Next, we considered MAb capture of four SOS ΔCT variants: SOS (parent), SOS NFL I559P, SOS D197N+NT1-5 and SOS D197N. PG16 and CH01 captured SOS NFL I559P less effectively, consistent with weaker BN-PAGE shifts (Fig 7). Previously, NT1-5 reduced non-NAb capture, but did not affect NAb capture [17]. However, here we observed poor capture D197N+NT1-5 by all V2 MAbs (Fig 9). D197N mutant alone did not significantly affect capture, although it tended to weaker capture. This reflects the poor V2 binding to NT1-5 by BN-PAGE (Fig 8). Overall, we infer that the I559P and NT1-5 both disrupt V2 epitopes. VRC03 capture was equivalent for SOS and SOS NFL I559P but was close to background for the D197N-containing mutants. This suggests that the N197 glycan clashes with VRC03. Contrasting with previous data [17], 15e, 39F and 447-52D capture was comparable for all 4 mutants, although the D197N tended higher.

Next, we considered UNC and NFL. PGT145 only modestly captured both clones, suggesting that I559P is important for PGT145 binding to SOS NFL I559P (Fig 9). PG16 and CH01 capture was also poor, like SOS NFL I559P. However, VRC38 capture was apparently unaffected by the lack of gp120/gp41 cleavage. VRC03 capture was weak, as its quaternary epitope is evidently dependent on cleavage. Conversely, 15e and V3 capture was effective. Overall, we conclude that lack of cleavage reduces capture by some V2 MAbs and those that depend on quaternary conformation.

PGT145, CH01 and VRC03 failed to capture SOS NFL A433P and SOS D197N+A328G mutants, consistent with “globally sensitive” phenotypes. PG16 and VRC38 captured A433P moderately, but not D197N+A328G. Both mutants were well-captured by 15e, 39F and 447-52D, albeit to differing extents. Overall, we infer that both mutants adopt tier 1 conformations, but with distinct antigenic profiles [10,70]. Lastly, there was no detectable CR3022 capture, indicating the specificity of the assay (S10B Fig).

I559P reduces HIV+ plasma recognition

In a previous study, 3 HIV-1 seropositive (HIV+) donor plasmas bound more strongly to WT than SOS I559P membrane Envs [38]. We extended this analysis by testing the binding of 22

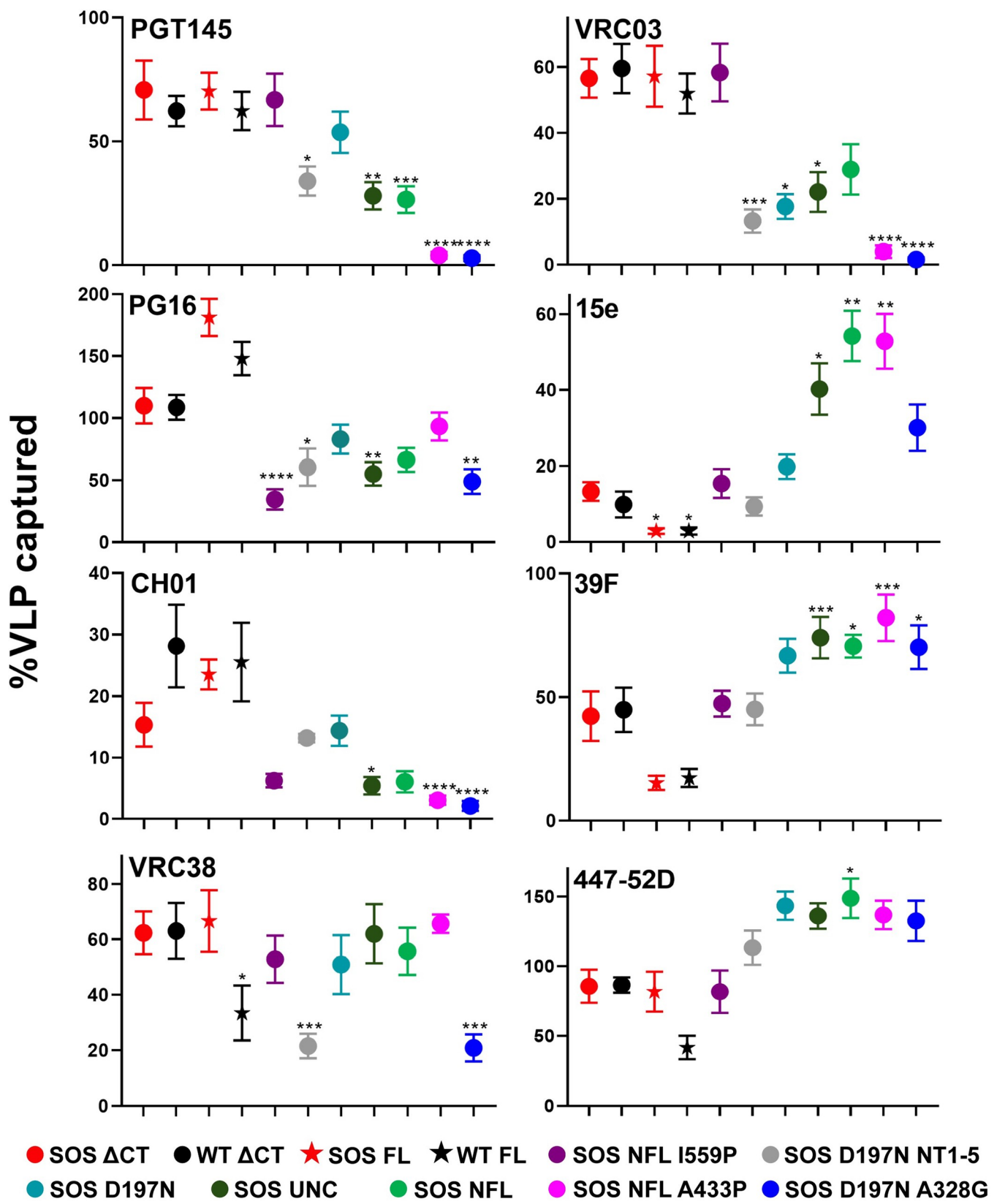


Fig 9. Antigenic profile of VLPs carrying different mutations assessed by virus capture assay. Capture of various JR-FL mutant VLPs by a subset of MAbs. For each mutant, data was normalized by 2G12 capture which approximates Env expression. This allows mutants to be compared regardless of expression differences. Virus capture assays were performed in quadruplicate and repeated at least three times. Error bars represent the standard deviation of the mean. UNC is gp160ΔCT SOS E168K+K510S+R511S. Kruskal-Wallis test was used to analyze for significant difference of different VLPs captured by a MAb, relative to SOS ΔCT VLP. * $p < 0.05$, ** $p < 0.01$, *** $p < 0.001$, **** $p < 0.0001$.

<https://doi.org/10.1371/journal.ppat.1011452.g009>

HIV+ plasmas from chronic infections [69,71] to JR-FL WT, SOS and SOS I559P VLPs by ELISA. Exemplary ELISA titers are shown in S11 Fig. G12 bound to all 3 Env VLPs equivalently, suggesting comparable expression. 2G12 did not bind to MuLV Gag “bald” VLPs (S11 Fig). A HIV-1-negative plasma, 210 showed only background binding (S11 Fig). HIV+ plasma binding to SOS VLPs was weaker than to WT VLPs (Figs 10A and S11). This may be due to the lack of immunodominant gp41 stumps on SOS VLPs. In addition, weaker plasma binding to SOS I559P compared to SOS may be due to conformational differences, exemplified by reduced V2 bNAb reactivity to I559P.

The plasmas exhibited a wide range of NAb ID50s (Fig 10B) against JRFL WT gp160ΔCT. Although the NAb specificities of some sera was at least partially mapped (Fig 10B), we could not link the differences in VLP binding based on epitopes. However, we note that plasmas N308, 1686, and BB12 exhibited potent NAb ID50s ($>1:400$), more than half of which is ascribed to CD4bs NAb, all showed relatively large differences in binding to SOS I559P compared to SOS (9.3-, 4.2- and 6.8-fold; Figs 10B and S11). Although there was a significant correlation between NAb ID50s and binding titer ratio SOS:SOS I559P (Fig 10B), this was dependent on the potently neutralizing N308 plasma. The correlation was lost when this plasma was excluded. Overall, the reduced “total antibody” binding to SOS I559P suggests a generalizable reduction in binding to structures associated with I559P.

Effect of I559P and NFL mutations on diverse V2-sensitive Envs

We previously reported a panel of optimized V2-sensitive membrane trimers [22]. I559P and NFL mutants were made in three selected strains, namely Q23-17, T250-4 and WITO.33. Denatured VLP lysates were digested with or without endo H and analyzed by SDS-PAGE--Western blot (S12A Fig). Traces of fully endo H-sensitive gp160i were detected in all 3 clones. Gp160i is in fact consistent in many strains expressed in 293T cells (see S9 Fig in [46]). In all cases, band patterns were less clear than observed above for JR-FL. Q23-17 and T250-4 SOS parent clones showed similar expression and band patterns. Notably, gp160m and gp120 bands treated with endo H migrated as amorphous smears (S12A Fig, lanes 2 and 8). This contrasts sharply with JR-FL, in which endo H treated gp120 and gp160m bands were far more distinct (Fig 3, lane 2). Perhaps revealingly, the endo H digested Q23-17 and T250-4 smears better resemble the misfolded DS mutant (Fig 3, lane 6). By comparison, WITO.33 was better expressed, but band patterns were even less clear after endo H digestion (S12 Fig, Lane 14).

In Q23-17 and T250-4, gp120 and gp41 bands were reduced by I559P (S12A Fig lower panel, compare lanes 1, 3, 7 and 9). In the case of T250-4, the I559P mutant expressed relatively poorly, while expression was not affected in Q23-17. Densitometry of gp160 and gp41 bands revealed I559P reduces gp120/gp41 processing of both strains (S12B Fig), supporting the general observation that I559P’s rigidifying effect that also blocked gp160 processing in JR-FL (Fig 3, lanes 3 and 4). On the other hand, WITO.33 I559P led to reduced expression to both gp160 and gp41 but did not appear to appreciably affect gp160 processing (S12B Fig, gp160:gp41 ratio = 1.24).

As expected, overlaying NFL reduced the gp41 band further in Q23-17 and T250-4, but the bands did not disappear completely (S12A Fig, lanes 5 and 11). In contrast, WITO.33 with NFL + I559P expressed better than I559P alone (S12A Fig, compare lanes 17 and 15). The

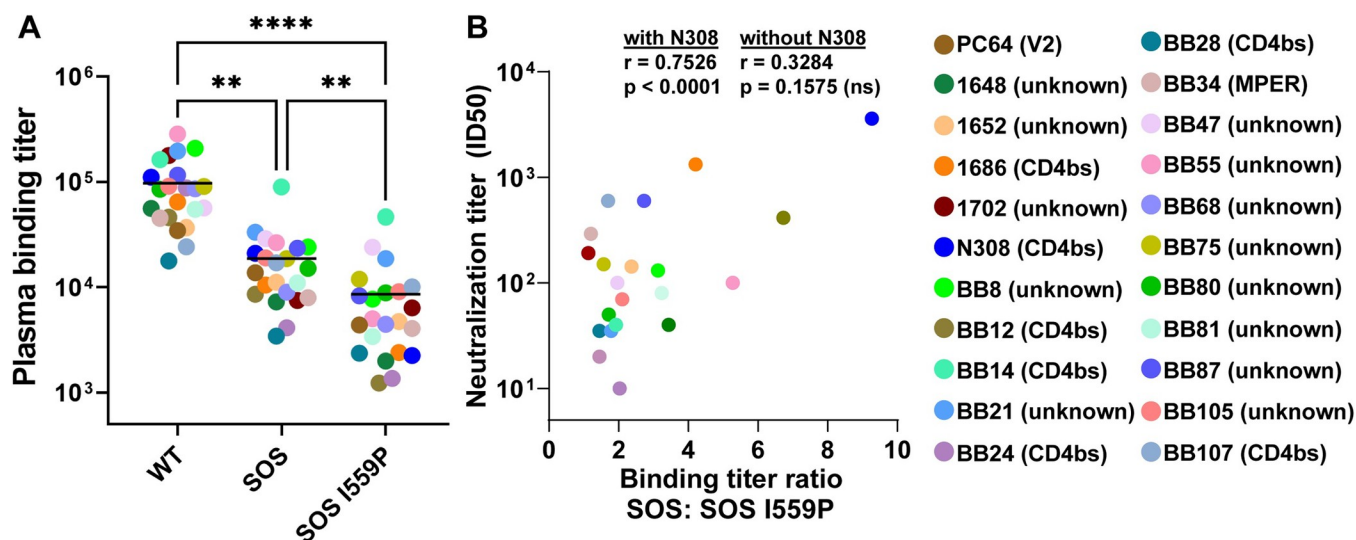


Fig 10. JR-FL gp160 Δ CT E168K+N189A VLP binding titer of human HIV+ plasma probed by VLP ELISA. (A) Plasma binding titer of human HIV+ plasma ($n = 22$) to JR-FL gp160 Δ CT WT, SOS or SOS I559P VLP analyzed by ELISA. Plasma binding titers were calculated as the dilution where its binding OD was 0.5. Geometric mean binding titer (GMT) against each VLP is indicated as horizontal line. One-way ANOVA Dunn's multiple comparison test revealed a significant difference of plasma binding titer between WT, SOS and SOS I559P VLPs. ** $p < 0.01$, **** $p < 0.0001$. (B) Correlation analysis of HIV+ plasma neutralization titers (ID50) against JR-FL gp160 Δ CT PV and binding titer ratio SOS:SOS I559P VLP. Correlation was significantly dependent on the highly neutralizing N308 plasma ($p < 0.0001$). The correlation was not significant when this plasma was excluded. Plasma NAb specificities, where known, are indicated in parentheses.

<https://doi.org/10.1371/journal.ppat.1011452.g010>

gp120/gp41 processing in WITO.33 NFL + I559P was less affected compared to Q23-17 and T250-4 with the same mutations (S12B Fig, compare gp160:gp41 ratio of WITO.33 to Q23-17 and T250-4). Overall, while the gp160m heterogeneity in these strains cloud the effects of I559P, reduced gp160 processing was evident for Q23-17 and T250-4.

Glycan analysis

To better understand the effects of JR-FL mutants, we assessed glycan occupation and maturation by glycopeptide in-line liquid chromatography mass spectrometry (LC-MS) [22,72,73]. In a previous study [22], we used this method to analyze unfractionated “total VLP” samples, in which the resulting data derives from the sum of various forms of Env that we described above in Western blots, including gp120/gp41 trimers, gp160m, gp160i and gp41 stumps. To generate “cleaner” samples for analysis and to enable us to discriminate between the glycan profiles of different Env isoforms, we ran VLPs on reducing SDS-PAGE and cut out bands for analysis. In the case of the parent VLPs, we cut out 3 bands corresponding to gp160 (including gp160m and gp160i bands, which run so close together that they could not be cut separately), gp120 and gp41. For the other samples (NFL, NFL I559P and NFL A433P), we cut out gp160 bands (gp160m and gp160i), as there are no gp120 and gp41 bands when the NFL is used.

Detailed glycopeptide data is provided in S1 File, containing a file for each sample. Data was obtained for all samples except for the gp41 band of the parent VLP, which was insufficient for detection. Data is plotted in bar charts (S13 Fig) that reveal the relative percentages of oligomannose, hybrid, complex and core glycans at each site, as well as unoccupied “skipped” sequons. These charts also show fucosylated and sialylated glycans (NeuAc/NeuGc) at each site.

To summarize the data and facilitate comparisons, each glycan type was given a score from 1 to 19, depending on the average maturation state (S1 Main glycan analysis). Specifically, the

high mannose glycan, M9Glc, has a score of 1, while the most highly branched and fucosylated complex glycan HexNAc(6+)(F)(x) has a score of 19. Glycans at each site were then given an overall score based on the presence of each glycoform at each site multiplied by its percent prevalence and rounded to the nearest whole number. Overall glycan scores were computed in [S1 Main glycan analysis](#) for each clone and are color coded for clarity. Glycan data were modeled for the viral gp160 bands ([S14A Fig](#)) and the viral gp120 band ([S14B Fig](#)) of the VLP parent. We also modeled parent “total VLP” samples (2020, 2021 and 2023) and gp120 monomer (2020) [22] ([S14C, S14D, S14E and S14G Fig](#)). Mutant glycan data were also modeled ([S15 Fig](#)). Glycan positions are based on HXB2 numbering.

To determine the effects of mutations on glycans, we first need to select a reference. The profiles of the 3 independent parent “total VLPs” (2020, 2021 and 2023) ([S13C–S13E](#) and [S14C–S14E](#) Figs and [S1 Main glycan analysis](#) “Scores and score change” worksheet) were largely similar. However, data for some glycan positions were missing in some preparations but present in others. Therefore, we decided to combine and average the parent data as a reference for the mutants ([S13F](#) and [S14F](#) Figs and [S1 Main glycan analysis](#) “Scores and score change” worksheet).

We next compared the glycan profiles of gp160 bands (containing gp160m and gp160i) and gp120 bands with each other and to the average parent as well as gp120 monomer ([S14G Fig](#)). Glycan score changes at each position are determined by subtraction. Score changes are color coded according to glycan processing: decreased processing is shown in shades of red and increased processing is shown in shades of blue ([Fig 11](#)). For clarity, we refer to VLP gp120 as viral gp120 to distinguish it from gp120 monomer. There were stark differences between viral gp120 and gp160 bands, particularly at N356, that was completely flipped to complex in viral gp120. Increased viral gp120 glycan maturation was also found at N88, N188, N392 and N463. These are modeled in [Fig 11A](#), summarized in [S1 Main glycan analysis](#) and shown in detail in [S1 Table](#).

Notably, viral gp120 did not show any sequon skipping ([S13B Fig](#)). This contrasts with viral gp160 bands, where there was partial skipping at N188 and N339 (gray shading in [S13A Fig](#) and [S1 Main glycan analysis](#)). Total VLP samples also exhibited detectable skipping ([S13C–S13E Fig](#)). Mutant gp160s exhibited enhanced skipping, particularly at N637 ([S13G–S13I Fig](#)). In addition, the mutants exhibited reduced glycan maturation at some positions (covered in detail below), coupled with reduced overall levels of sialylation and fucosylation ([S13 Fig](#), compare part F to parts G–I). Comparing viral gp160 ([S14A Fig](#)) to the parent average ([S14F Fig](#)) also revealed reduced glycan maturation at the same positions ([S1 Table](#)). In contrast, the glycan profiles of the parent average and viral gp120 ([S14B Fig](#)) were more consistent ([S1 Main glycan analysis](#) and [S1 Table](#)).

If viral gp120 and gp160m express equivalently, one might expect increased diversity at the variable glycan sites in total VLPs, as they would reflect the combined diversity of both gp120 and gp160m components ([S1 Table](#)). To some extent, this is the case at N188 and N463 (especially the parent “total VLP” 2023 sample), but not so much at N88 and N356 that was biased more towards viral gp120 profile. In the parent “total VLP” 2023 sample, N392 exhibited intermediate processing. Overall, this suggests that functional gp120/gp41 trimers are the predominant form of Env in total VLPs and gp160m is the weaker form. Furthermore, the near complete complex glycans at some positions suggests that gp160m dominates over gp160i, which exhibits high mannose glycans at all positions [46].

The gp120 monomer profile at variable positions N88, N160, N356 and N463 was also more akin to viral gp120 than the gp160 bands ([S1 Table](#)). However, the glycan at N392 was far more processed on gp120 monomer than on viral gp120 or total VLPs ([S1 Table](#)). We therefore infer that N392 is uniquely buried in native trimers.

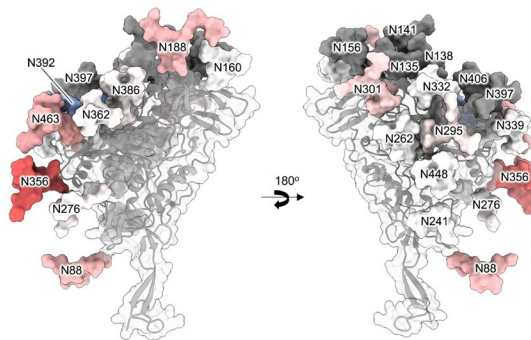
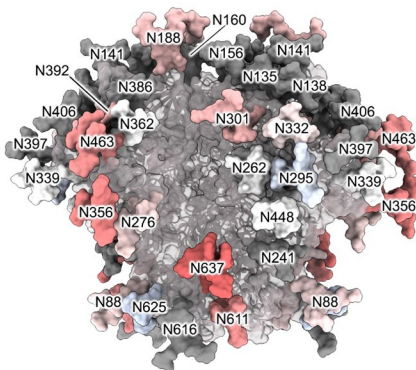
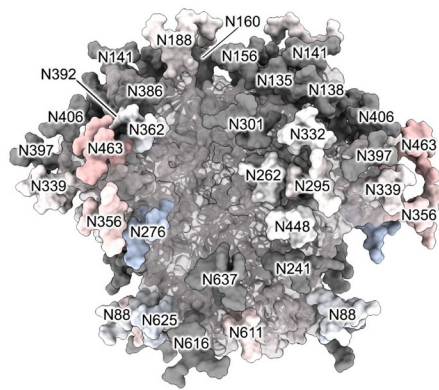
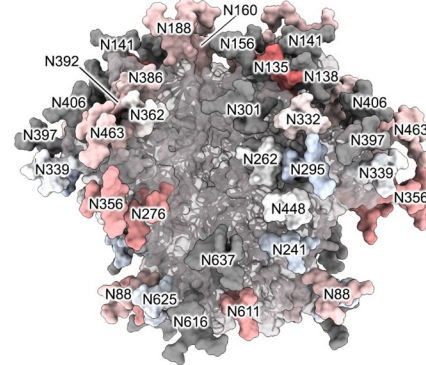
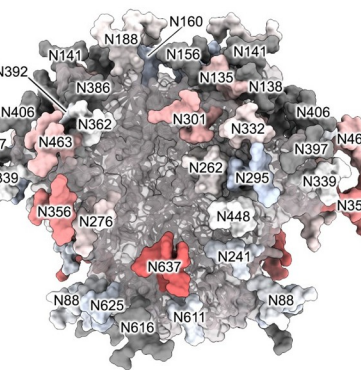
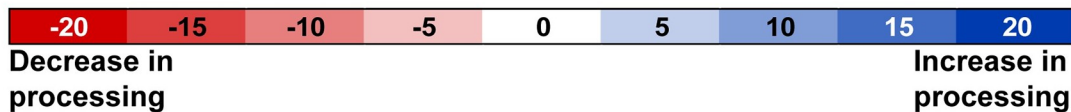
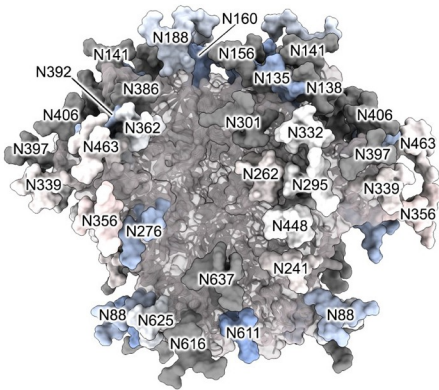
A. Viral gp120 2023 vs Viral gp160 2023**C. Parent average* vs SOS NFL I559P VLP (gp160 bands)****E. SOS NFL VLP (gp160 bands) vs SOS NFL I559P VLP (gp160 bands)****B. Parent average* vs SOS NFL VLP (gp160 bands)****D. Parent average* vs SOS NFL A433P VLP (gp160 bands)****F. SOS NFL VLP (gp160 bands) vs SOS NFL A433P VLP (gp160 bands)**

Fig 11. Effects of NFL, I559P and A433P mutants on gp160 Δ CT glycan maturation and occupation. Related to S13–S15 Figs and S1 Main glycan analysis and S1 File. Each glycan on the trimer models (pdf: 6MYY) is numbered according to HxB2 strain and is given a maturation score derived from LC-MS analysis. Glycan score differences between two clones are colored in shades of red (i.e., a negative score indicates decrease in processing), white (no difference in glycan processing) or blue (i.e., positive score indicates increase in processing). Data are only shown at positions where a glycan was detected in >10% of the equivalent peptides

of both samples in each pair. Some glycans, rendered in gray, were not resolved in the sample, and therefore have no score (not done; n.d.). Glycan score difference calculations between sample pairs are shown in [S1 Main glycan analysis](#), and are modeled here as follow: (A) Viral gp120 band vs viral gp160 bands; (B) Parent average vs SOS NFL VLP gp160; (C) Parent average vs SOS NFL I559P VLP gp160; (D) Parent average vs SOS NFL A433P VLP gp160; (E) SOS NFL VLP gp160 vs SOS NFL I559P VLP gp160; (F) SOS NFL VLP gp160 vs SOS NFL A433P VLP gp160. *Parent average is the glycan score average of “total VLPs” preparation from 2020, 2021 and 2023 ([S14F Fig](#)).

<https://doi.org/10.1371/journal.ppat.1011452.g011>

Mutant glycan profiles compared to parent

The key information we sought here is whether mutants affect glycan compositions, as an indicator of conformational differences. We therefore compared the parent average to NFL, NFL I559P and NFL A433P ([Fig 11B–11D](#) and [S1 Main glycan analysis](#)). SDS-PAGE data above indicated that I559P bands were fast moving and slightly more endo H sensitive, whereas A433P bands were slightly slower moving ([Fig 2](#)). We hoped that glycan analysis would help us to reconcile these effects.

All 3 mutants trended towards reduced glycan processing ([S1 Main glycan analysis](#) “Scores and score change” worksheet). This implies that the lack of gp120/gp41 cleavage is one contributor to variant glycan profiles. However, there are differences between mutants. First considering NFL, the most profound reductions in glycan processing occurred at N135, N276, N356, and N611. The latter is unusual, as the 4 gp41 glycans are usually all heavy and complex. Notably, the N637 was completely unoccupied in NFL and was only partially occupied in the other mutants ([S13G–S13I Fig](#)). N611 was also poorly processed in I559P but not A433P, consistent with increased I559P gp160 endo H-sensitivity ([Fig 3](#)). This suggests that gp41 glycan sites are poorly accessible prior to gp120/gp41 processing. N463 was also unusually underprocessed in I559P. I559P’s generally poor glycan maturation may explain the increased 35O22 binding in BN-PAGE ([Fig 7C and 7D](#), lane 14), as glycan clashes are reduced when glycans are smaller in size. This is akin to the improved 35O22 sensitivity of GnT1-modified pseudovirus, where glycan clashes are reduced [46].

Mutant glycan profiles compared to NFL

By comparing to NFL, the effects of I559P and A433P can be understood independently ([Fig 11E and 11F](#) and [S1 Main glycan analysis](#)). Both mutants increased N276 glycan processing, rescuing the glycans closer to the maturation state of the parent. N88, N160, N188, and N392 were well-differentiated in A433P, perhaps due to an open trimer conformation and could account for the decreased mobility of A433P clones in SDS-PAGE ([Fig 2](#), lane 5). If A433P is a more “open” trimer, it makes sense that N160 is more processed as it is on gp120 monomer, where there are no constraints. N392 also appears to be regulated by compactness, as discussed above.

The most important difference is the N611 glycan, which for I559P is less differentiated but is restored to a complex glycan in A433P. Data for gp41 glycans at positions 616 and 637 were not available due to proximity to N611 and/or skipping, but N625 is complex and appears unaffected by the mutations. Thus, the higher endo H sensitivity of I559P appears to be partly explained by dramatically reduced glycan maturation at N611 and N637.

We observed a decrease in the fucosylated glycans in I559P compared to A433P ([S13H–S13I Fig](#)). However, all mutants showed overall fewer fucosylated glycans than the average parent. This may simply reflect reduced glycan processing and the resulting bias towards high mannose glycans that do not exhibit terminal modifications.

Finally, we noted that N301 glycan is an outlier in its variable maturation between samples. It showed a score of 10 in the parent “total VLP” 2023 sample, 17 in 2021 and was not detected

in 2020 sample. Previous data suggests that this glycan is prone to “flipping”. It is often of complex type in viral Env and high mannose in soluble SOSIP [74]. Although viral gp160 showed the lowest score of 4 at N301, viral gp120 and gp120 monomer had intermediate scores of 8 and 7, respectively, so it is difficult to make an argument based on accessibility or else the gp120 monomer would show increased processing. The two mutants A433P and I559P also showed scores of 7, adding to this paradox. Overall, this suggests that it is subject to high variability in different preparations of the same sample, perhaps indicating a stochastic process.

Discussion

Functional Env folding involves trimerization, glycan addition and maturation, chaperone engagement, disulfide isomerization, signal peptide removal and gp120/gp41 processing. Given this complexity, a modicum of misfolded Env is perhaps inevitable. How gp160i avoids glycan maturation in the ER/Golgi is currently unknown. Revealingly, none of our mutants impacted gp160i, consistent with it being an early misfolding product that exits conventional folding before mutants can have an effect. Our BN-PAGE analysis showed that uncleaved forms of Env, including UNC, NFL, gp160m and gp160i are largely monomeric. In contrast, we recently observed that nascent gp160 extracted from cell lysates is *entirely* trimeric [28]. The reasons for this dichotomy are unclear. Possibly, trimers are stabilized by cellular factors in lysates that are largely absent by the time Env reaches the outer cell membrane. Pretreating VLPs with a crosslinker prevented some but not all UNC trimers from laterally dissociating. In contrast, cleaved trimers gained sufficient lateral stability to survive lysis.

UNC’s lateral instability may be linked to its conformational flexibility. A recent study used crosslinkers to characterize two asymmetric UNC isoforms [27]. Indeed, expression of gp160 in the presence of BMS-806, an entry inhibitor that binds the Phe43 cavity and promotes a “state 1” conformation, reduces gp120/gp41 processing and glycan maturation [27]. Here, I559P, DS and NT1-5 also reduced or eliminated gp120/gp41 processing. I559P and NT1-5 led to increased trimer, coupled with reduced monomer in the case of NT1-5. The poor gp120/gp41 processing of these mutants suggest that reducing UNC flexibility improves lateral trimer stability. I559P improved Env expression appears to be common for proline mutants [75].

Our glycopeptide data raise a key question of whether viral gp120 and gp160 glycan differences occur before or after gp120/gp41 processing. In this regard, uncleaved NFL is instructive. At N356, NFL gp160 glycans were more mixed than the average parent (which is biased to native trimers) or viral gp120 ([S1 Main glycan analysis](#)). At N392, NFL was largely oligomannose, unlike viral gp160, but more consistent with the average parent. This suggests the presence of a native-like conformation within NFL gp160 that would have been gp120/gp41 processed had the cleavage site had been intact. Moreover, it suggests that glycan maturation differences precede gp120/gp41 processing. Further, it suggests the presence of at least two gp160 populations in NFL, a dominant fraction that is folded and another that is misfolded and undergoes different glycan processing. Said another way, this implies that protein folding, not gp120/gp41 cleavage dictates glycan maturation. This does not exclude possible late maturation of some glycans, most notably of gp41 in which some high mass complex glycans may develop only after gp120/gp41 cleavage.

Compared to native parent Env trimers ([S13C–S13F Fig](#)), mutants ([S13G–S13I Fig](#)) exhibited sequon skipping and overall decreased glycan processing, fucosylation and sialylation. This resembles previous comparisons of soluble SOSIP and viral glycans, where soluble SOSIP also exhibited skipping and decreased glycan differentiation [72,74]. This suggests that mutants consistently disrupt glycosylation in both soluble and membrane trimer formats. Mutants all showed large changes in gp41 glycans and increased skipping, especially at N637.

As immunogens, these non-encoded glycan holes could draw Abs to an irrelevant target. Overall, these findings suggest a scenario in which glycans progressively mature as gp160 disulfides isomerize and exchange until they reach the canonical native conformation, by which point glycans are most differentiated. This is consistent with previous observations that live HIV-1 is heavily sialylated [46,72,76,77]. A less mature glycan profile may therefore signify aborted attempts to reach the final native conformation and may be a marker of misfolding.

How broadly applicable are the phenotypes we observed with JR-FL mutants?

Most of our work used JR-FL, which we originally selected for its high level of gp120/gp41 processing, high expression and infectivity. The question arises if these findings apply generally to other strains. Despite the heterogeneous band patterns and poor gp160 processing of the parent strains, it appears that 2 out of 3 other strains (Q23-17 and T250-4) showed reduced processing. Another study showed that BG505 I559P is poorly processed and causes antigenic changes [38]. Overall, I559P often reduces gp160 processing. This is not surprising given that the objective of I559P is to stabilize trimers laterally, which runs against the idea that gp160 must be flexible to reach its mature conformation. Further addressing the broad applicability of mutants, SOS in PC64 MRCA increased V3 sensitivity. In a previous paper, we also observed that SOS can exacerbate slight V3 sensitivity of parent strains [22].

How do mutants affect antigenicity and glycans?

We consider the antigenicity of each modification below.

Gp41 N-helix mutations. Given its adverse effect on gp120/gp41 processing, it is perhaps no coincidence that I559P is frequently used in conjunction with gp120-gp41 linkers, ostensibly to achieve a “native like” conformation. The antigenic profile of I559P and NT1-5 showed some differences from parent trimers, most clearly for V2 and interface bNAbs, consistent with other studies [33,38–40]. Although some V3 non-NAb epitopes are partially exposed on soluble SOSIP trimers [33], we did not see differences in membrane trimers: V3 MAbs did not bind to either parent or I559P trimers in BN-PAGE, but VLPs were captured equivalently by V3 MAbs, presumably via non-functional gp160m. Lastly, UFO significantly reduced membrane trimer expression. A recent study showed that incorporating both gp120-gp41 linker and UFO into a Clade C soluble gp140 resulted in low trimer expression and reduced V2 NAb binding [78]. The same mutations, when applied to another soluble Env, resulted in a higher trimer expression [10], suggesting that UFO and NFL are not universally compatible.

The modest but significant 2.2-fold reduced HIV+ plasma binding to I559P (Fig 10), suggests globally diminished Ab reactivity across multiple epitopes. Extrapolating this in a vaccine setting, I559P trimers are likely to induce some I559P-specific Abs that inefficiently cross-react with native trimers, thereby blunting potential NAb titers and reducing vaccine efficacy.

The most notable feature of I559P’s glycan profile was its greatly decreased processing at N637 and to a lesser extent at N611. This may be due to the self-association of gp41 C-helices that results in reduced accessibility for glycan processing enzymes. Furthermore, glycan skipping was observed to varying degrees at N637 in NFL+ mutants, whereas all gp41 glycans are complex in the parent. The mutations therefore create non-encoded glycan holes, like that reported in BG505 gp140 SOSIP trimer where low glycan occupancy was observed at position 611 [79]. Immunogens with such glycan holes trigger autologous Ab responses that are unable to cross-react with membrane Envs that lack glycan holes [80].

We note that some mutations directly ablate epitopes rather than mediate conformational improvement. For example, UFO may directly ablate gp41 cluster I or II non-NAb epitopes,

rather than eliminate them conformationally. Hence, the lack of binding by these MAbs does not imply the Env adopts a more native conformation. Similarly, given its proximity to the 17b epitope, A433P may directly knock out 17b binding rather than prevent CD4-induced conformational change.

DS. The DS mutant did not stabilize the native-like membrane trimers and lacking sCD4 binding constraint suggests that the disulfide may not form as intended [36]. One explanation is that, like I559P, NT1-5 and UFO, DS diminishes UNC's flexibility that is crucial for attaining correct disulfide bonding and gp120/gp41 processing [10,52]. The DS mutant was designed based on soluble SOSIP structure that conformationally differs from membrane trimers, such that positions 201 and 433 may not be proximal [31]. These cysteines may instead react with others to form non-canonical disulfides, possibly accounting for dimers and the heterogenous gp160m glycans.

A433P. A433P caused a globally sensitive phenotype like A328G, eliminating PGT145 binding and increasing V3 MAb and CD4bs non-NAb binding. Its “open trimer” conformation led to increased glycan maturation at several variable positions, namely N88, N188, N276, N392, and N611. However, like I559P and NFL, position 637 was often skipped and/or confined to oligomannose, contrasting sharply with the parent. Therefore, N637 is commonly impacted by mutations, perhaps as its position proximal to the viral membrane can dramatically impact its accessibility to glycan processing enzymes.

Globally sensitive mutants like A433P and A328G are ubiquitous among membrane Env point mutants [40,81,82] and appear to reflect misfolding. These mutants show reduced trimer in BN-PAGE, suggesting that globally sensitive trimers are laterally labile. Although I559P “rescued” A433P trimers, dimers also became prominent, suggesting misfolding.

SOS and ΔCT. Gp120 shedding appears to occur largely as a by-product of trimer synthesis, at least for primary isolates. We suggest that a fraction of misfolded Env is somehow processed into gp120/gp41, but due to misfolding, lacks sufficient cognate gp120-gp41 non-covalent associations, so gp120 immediately dissociates [83]. This leads to the exposure of gp41 stumps which are highly immunogenic and likely account for the greater HIV+ plasma reactivity with WT over SOS membrane Env (Fig 10). To try to force a greater focus on NAb epitopes, we have used SOS in multiple vaccine studies [25,26,84]. SOS appears to improve trimer expression, which may simply be due to the retained gp120. Overall, the mild antigenic cost of SOS may be less important than eliminating immunodominant gp41 epitopes.

Our previous vaccine studies used ΔCT due to increased gp160 processing and increased expression. In the context of JR-FL, neutralization sensitivity is largely unchanged by either SOS or ΔCT. In other studies, ΔCT also did not affect NAb sensitivity [33,36,38]. However, in some contexts, these mutations cause unwanted increases NAb sensitivity, i.e., misfolding [85]. While the full gp41 tail may be linked to a compact trimer apex, as evidenced by enhanced PG16 capture (Fig 9), an important caveat of FL for vaccine use is its extremely poor gp120/gp41 cleavage.

We were intrigued that FL gp160 was not *detectably* bound by MAbs in BN-PAGE (Fig 8C). This must be reconciled with the fact that the *same* MAbs can capture FL VLPs. Other BN-PAGE shifts reveal a similarly puzzling lack of MAb binding to the monomer (Fig 7). We suggest that lack of MAb binding to trimers and monomers are linked. It may be no coincidence that FL is very poorly cleaved and expresses unusually high levels of gp160i compared to ΔCT clones (S4 Fig). Gp160i partly accounts for BN-PAGE monomers in all cases. Given the predominance of gp160i over gp160m and gp120/gp41 in FL clones (S4 Fig), gp160i may also significantly account for the FL trimer in BN-PAGE. We further suggest that MAb binding to gp160i on intact VLPs is prevented by gp160i complexing with host chaperones that might be linked to its trafficking to cell supernatants. These complexes may be held together by low

affinity interactions that, upon VLP lysis, become dissociated, thereby allowing MAbs to bind (Fig 8). Despite this, FL VLPs exhibited traces of functional trimer and non-functional Env that presumably is not complexed to chaperones, thereby allowing virus capture and neutralization, contrasting with BN-PAGE that is dominated by gp160i.

Gp120-gp41 linkers. One argument for the use of gp120-gp41 linkers in vaccines is that cellular furin processing is almost invariably incomplete, leading to a heterogeneous product. However, our glycan data suggests that despite controlling cleavage, the resulting product is not uniform. Instead, some gp160 gains glycans similar to native trimers, while other gp160 is less differentiated. In short, eliminating cleavage heterogeneity does not eliminate glycan heterogeneity. Thus, “native glycan” trimers will be arrayed alongside less differentiated trimers. Multivalent vaccines such as measles, mumps, rubella (MMR) demonstrate that multiple Ab lineages can develop to distinct antigens in parallel. However, it is unknown how similar but non-identical trimer isoforms might influence Ab responses to each other, although it is almost inevitable that the more Ab-sensitive trimers will dominate. By analogy, glycan holes are preferential Ab targets and may delay NAb development [86,87]. For similar reasons, gp160-expressing mRNA vaccines have so far been only moderately successful [52], perhaps because non-functional Env and/or mutations create antigenic differences so that Abs insufficiently cross-react with native trimers.

What features and modifications do we recommend for membrane trimer vaccines?

Our long-standing goal is to develop a vaccine that expresses *fully* cleaved trimers—unfettered by UNC [36,39,64]. Such immunogen has yet to be tested. Our stepwise suggestions to effectively present native trimers are as follows:

- *To select epitope-sensitive strains for use in immunofocusing.
- *To modify sequence as needed to fill any off-target glycan holes and/or to correct any aberrant sequence (indels, rare sequence stretches) especially in gp120 constant domains by aligning to multiple reference strains.
- *To perform an expression check to weed out poorly expressing clones.
- *To perform a V3 MAb neutralization sensitivity check to weed out “open” trimers that don’t resemble primary HIV-1 isolates.
- *To prioritize clones that i) express high levels of mature glycans and ii) show effective gp160 processing.
- *To optimize target epitope sensitivity and also create epitope variant boosts including glycan variants to promote broad NAb cross-reactivity.
- *To find ways to ensure the expression pure native gp120/gp41 trimers.

Of the stabilizing mutants, we suggest using SOS only when V3 MAb resistance is intact. SOS prevents the development of immunodominant gp41 stump Ab responses. We do not recommend using I559P, NT1-5, NFL, UFO, A433P or DS. These stabilizing mutants provided structural insights and advanced soluble trimer vaccine designs. However, none of them are helpful in the context of membrane Env if the goal is to present native Env spikes. Indeed, we previously found that other soluble trimer mutations are also unnecessary in membrane context [22]. Overall, if successful, we hope that membrane Env expressed by nucleic acid vaccines can induce bNAbs, as occurs commonly in natural HIV-1 and SHIV infections [88].

Materials and methods

Plasmids

i) Env. Abbreviated Env strain names are given first, with full names and GenBank references in parentheses: JR-FL (JR-FL, AY669728.1), Q23 (Q23.17, AF004885.1), WITO (WITO.33, AY835451.1), T250 (also known as CRF250 or T250-4, EU513189.1), PC64 (PC64 MRCA, ASP69831.1). These were expressed in plasmids pCDNA3.1 (PC64 MRCA, T250-4, WITO.33), pVRC8400 (Q23-17) or pCAGGS (JR-FL). All gene synthesis, cloning and mutagenesis was performed by GenScript (USA). Amino acids are numbered according to the canonical HXB2 subtype B reference strain.

ii) Gag and Rev. A plasmid expressing murine leukemia virus (MuLV) Gag was used to produce VLPs [62]. For Env plasmids using native codons, we co-transfected pMV-Rev 0932 that expresses codon-optimized HIV-1 Rev.

iii) NL4-3.Luc.R-E. This plasmid is based on HIV-1 proviral clone NL4-3 in which the firefly luciferase gene replaces Nef and does not express Env or Vpr due to frameshift mutations. This plasmid is co-transfected with Env plasmids to produce pseudovirions (PVs) for neutralization assays.

iv) VSV-G. A plasmid expressing vesicular stomatitis virus G protein described previously [85] is used as a readout of capture virus capture assays.

v) pQC-Fluc-dIRES and pMLV GagPol. These two plasmids express luciferase and Gag-Pol respectively, for use in the alternative pQC-Fluc neutralization assay format.

MAbs and soluble CD4

MAbs were obtained from their producers or the NIH AIDS Reagent Repository. These included PGT145, PG16, CH01, VRC38.01 and PC64 35K, directed to the V2 apex; 14E, 39F, 447-52D and CO11, directed to the V3 loop; 2G12 and PGT121, directed to V3-glycan epitopes; VRC01, VRC03, b12 and 15e, directed to the CD4 binding site (CD4bs); 17b, directed to a CD4-induced epitope/bridging sheet; PGT151, 35O22 and VRC34, directed to the gp120-gp41 interface [89]; 2F5, 4E10, 10e8, 7B2 and 2.2B directed to gp41 and CR3022 directed to SARS-CoV S. Four-domain soluble CD4 (sCD4) was provided by Progenics Pharmaceuticals, Inc.

HIV+ donor plasmas

A collection of HIV-1+ plasmas we and others previously described [71] were obtained from various subtype B- and C-infected donors. Four subtype B plasmas, from United States donors 1648, 1652, 1686, 1702 and an uninfected donor (210) were obtained from Zeptometrix (Buffalo, NY). N308, a long-term nonprogressor B plasma was described previously [90]. Subtype C plasmas were purchased from the South African Blood Bank (Johannesburg). PC64 plasma was from a subtype A infected donor, provided by Elise Landais [69].

VLP production

For VLP production, Env plasmids were co-transfected in human embryonic kidney 293T cells using polyethyleneimine (PEI Max, Polysciences, Inc.), along with the MuLV Gag plasmid and pMV-Rev 0932 for Envs carrying native codons. 48h later, supernatants were collected, precleared, filtered, and pelleted at 50,000g. Pellets were washed with PBS, reconstituted in a microcentrifuge at 15,000rpm, and resuspended at 1,000x the original concentration in PBS.

Endoglycosidase H (Endo H) and enterokinase digests

For endo H digests, VLPs were mixed with 2% SDS and 2-mercaptoethanol and boiled for 5 minutes. Samples were then split in half. To each sample, 2 μ l of endo H (1000U) (New England Biolabs) or 2 μ l of PBS (mock) were added and samples were incubated at 37°C for 15 minutes. Samples were then lysed and processed for SDS-PAGE-Western blot.

For enterokinase (EK) digests, VLPs were mixed with rEK 10x cleavage buffer and were digested with 1 μ l of enterokinase (equivalent to 2.4U; Novagen) at 37°C for 30h. Samples were then lysed and processed for reducing SDS-PAGE-Western blot.

SDS-PAGE-Western blots

VLPs were denatured by heating in 2xLaemmli buffer containing 2-mercaptoethanol (Bio-Rad) for 10 minutes at 95°C, and proteins were resolved in 4–12% Bis-Tris NuPAGE gel (ThermoFisher). Proteins were wet transferred onto a PVDF membrane and blocked in 4% skim milk/PBST. Blots were probed for 1h at room temperature with MAb cocktails in 2% skim milk/PBST, as follows (epitopes in parentheses). Anti-gp120 MAb cocktail: 2G12 (glycan), b12 (CD4bs), 39F (V3 loop), PGT121 (N332 glycan), 14E (V3 loop). Anti-gp41 MAb cocktail: 2F5 (membrane proximal ectodomain (MPER)), 4E10 (MPER), 7B2 (cluster I), 2.2B (cluster II). After washing, blots were probed with a goat anti-human IgG alkaline phosphatase (AP) conjugate (Accurate Chemicals) at 1:5,000 in 2% skim milk/PBST for 30 minutes at room temperature. Following washing, protein bands on the blots were developed with chromogenic substrate SigmaFast BCIP/NBT (Sigma). All blots were run at least twice to check for reproducibility. Representative data is shown.

Blue Native (BN) PAGE-Western blots

VLPs were solubilized in 0.12% Triton X-100 in 1mM EDTA. An equal volume of 2x sample buffer (100mM morpholinepropanesulfonic acid (MOPS), 100mM Tris-HCl, pH 7.7, 40% glycerol, and 0.1% Coomassie blue) was added. Samples were spun to remove any debris and loaded onto a 4–12% Bis-Tris NuPAGE gel and separated for 3h at 4°C at 100V. Proteins were then transferred to PVDF membrane, de-stained, and blocked in 4% skim milk in PBST. Membranes were probed with a cocktail of MAbs 39F, 2F5, b12, 4E10, 14E, and PGT121, followed by anti-human IgG AP conjugate (Accurate Chemicals) and were developed using SigmaFast BCIP/NBT. In some experiments, Env was cross-linked on VLP membrane surfaces, prior to lysis and BN-PAGE. For this purpose, the cross-linker bis(sulfosuccinimidyl) suberate (BS³) (Sigma) was used [30].

In BN-PAGE band shifts, VLPs were mixed with either sCD4 or a MAb (30 μ g/ml) for 1h at 37°C, followed by either washing with PBS to remove excess ligand (“Wash out” method) or no washing (“Leave in” method), and subsequent processing for BN-PAGE as above. Blots were probed in two ways: first we used anti-human IgG AP conjugate and developed the blot with substrate to check for any MAb bound to VLP Env. Next, we probed the same blot with MAb cocktail, as above, to detect Env on the blot, followed by anti-human IgG AP conjugate. Band densities were determined using ImageJ software v. 1.33u (NIH freeware; <http://rsb.info.nih.gov/ij/>). All blots were run at least twice to check for reproducibility. Representative data is shown.

Neutralization assays

All neutralization assays were performed at least twice.

i) NL-Luc assay. Pseudoviruses (PV) were produced by co-transfected 293T cells with pNL4-3.Luc.R-E and an Env plasmid using PEI Max. Briefly, PV was incubated with graded dilutions of MAbs for 1h at 37°C, then added to CF2Th.CD4.CCR5 cells, plates were spinoculated, and incubated at 37°C [46]. For SOS PV, following a 2h incubation, 5mM dithiothreitol (DTT) was added for 15 minutes to activate infection. All MAb/PV mixture was replaced by fresh media (i.e., a “washout” protocol), cultured for 3 days, and luciferase activity was measured using Luciferase Assay System (Promega).

ii) pQC-Fluc assay. PV were produced by co-transfected Env plasmids with pMLV Gag-Pol and pQC-Fluc-dIRES [22]. The resulting PV were used in neutralization assays with CF2Th.CD4.CCR5, as above.

Virus capture assay

The antigenic properties of Env on VLP surfaces was analyzed using virus capture assay [30,91,92]. Briefly, MAbs were coated on Immulon II ELISA plates (Corning, USA) overnight at 5µg/ml in PBS. Wells were washed with PBS and blocked with 3% bovine serum albumin (Sigma) in PBS. VLPs were then added to the plate and incubated for 3h, after which the wells were washed three times with PBS. Since our Env mutants were generally non-infectious, VLPs were made to co-express VSV-G. 293T cells were added to wells to measure captured VLPs that infect via amphotropic VSV-G. Infection was detected by luciferase assay, as for neutralization. Virus capture assays were performed at least twice.

VLP ELISA

ELISAs were performed as described previously [93]. Briefly, Immulon II ELISA plates were coated overnight at 4°C with VLPs at 20x their concentration in transfection supernatants. Following PBS washing and blocking with 4% BSA/PBS supplemented with 10% FBS at room temperature, MAbs and HIV+ human plasmas were titrated against VLPs in 2% BSA/PBS/10% FBS. Goat anti-human IgG AP conjugate and PNPP Substrate tablets (ThermoFisher) were used to detect binding. Plates were read at 405nm. MAb concentration and plasma dilution resulting in an optical density (OD) of 0.5 (approximately 5 times above background) was recorded as its binding titer. All ELISAs were performed at least twice to check for reproducibility. Representative data is shown.

Env reduction, alkylation and digestion for mass spectrometry

The following VLP samples were subjected to glycopeptide analysis: JR-FL gp160ΔCT SOS, SOS NFL, SOS NFL I559P and SOS NFL A433P. VLPs were denatured by heating in 4xLaemmli buffer containing 2-mercaptoethanol (Bio-rad) for 10 minutes at 95°C, then loaded onto 4–12% Bis-Tris NuPAGE gel. Western blot was carried out to determine the positions of gp160 (includes gp160m and gp160i), gp120 and gp41 on the gel and was used as “marker” to cut Envs from the gel. Gel slices containing either gp160, gp41 and/or gp120 were incubated in 500 µL acetonitrile (ACN) until opaque. ACN was then removed and replaced with 50 µL 10 mM DTT in 100 mM ammonium bicarbonate (AmBic). Gel slices were incubated in DTT solution for 30 minutes at 56°C. Gel pieces were cooled down and washed with 500 µL ACN, then incubated in the dark for 20 minutes in 50 µL 55 mM iodoacetamide (IAA) in 100 mM AmBic. Bands were then washed once with 500 µL 100 mM AmBic and ACN. Washed bands were then incubated on ice with either α-lytic protease, trypsin or chymotrypsin (13 ng/µL) in a solution of 10 mM AmBic 10% ACN. Further enzymatic solution was added and incubated on ice for another 90 minutes, ensuring the bands were fully submerged. 10–20 µL 10 mM AmBic was added, and the mixture was then incubated overnight at 37°C.

Following digestion, the gel pieces were spun down and supernatants were set aside in a fresh tube. The individual supernatants were dried using a heated vacuum centrifuge set to 30°C and resuspended in 200 µL 0.1% trifluoroacetic acid (TFA). The Oasis PRiME HLB 96-well µElution plate (Waters) was placed on a vacuum manifold set to 5" Hg. The HLB µElution wells were conditioned using 200 µL ACN, then equilibrated with 200 µL 0.1% TFA. The vacuum was turned off and the resuspended peptides were loaded into the conditioned wells. Vacuum was applied, starting at the lowest setting, and slowly increased to 5" Hg. Wells were washed with 800 µL TFA, followed by 200 µL H₂O to remove excess salts. The collection tray was placed in the vacuum manifold and peptides were eluted using 80% ACN in 0.1% formic acid. The eluted peptides were dried prior to LC-MS analysis using a heated vacuum centrifuge set to 30°C.

Liquid chromatography-mass spectrometry (LC-MS) glycopeptide analysis

Peptides were dried then resuspended in 0.1% formic acid and analyzed by nanoLC-ESI MS with an Ultimate 3000 HPLC (Thermo Fisher Scientific) system coupled to an Orbitrap Eclipse mass spectrometer (Thermo Fisher Scientific) using stepped higher energy collision-induced dissociation (HCD) fragmentation. Peptides were separated using an EasySpray PepMap RSLC C18 column (75µm × 75cm). A trapping column (PepMap 100 C18 3µM 75µM x 2cm) was used in line with the LC prior to separation with the analytical column. LC conditions were as follows: 280 minute linear gradient consisting of 4–32% ACN in 0.1% formic acid over 260 minutes, followed by 20 minutes of alternating 76% ACN in 0.1% formic acid and 4% ACN in 0.1% formic acid to ensure all the sample elutes from the column. The flow rate was set to 300nL/min. The spray voltage was set to 2.7 kV and the temperature of the heated capillary was set to 40°C. The ion transfer tube temperature was set to 275°C. The scan range was 375–1500 m/z. Stepped HCD collision energy was set to 15%, 25% and 45% and the MS2 for each energy was combined. Precursor and fragment detection were performed with an Orbitrap at a resolution MS1 = 120,000, MS2 = 30,000. The AGC target for MS1 was set to standard and injection time set to auto which involves the system setting the two parameters to maximize sensitivity while maintaining cycle time.

Site-specific glycan classification

Glycopeptide fragmentation data were extracted from the raw file using Byos (Version 3.5; Protein Metrics Inc.). Glycopeptides were evaluated in reference to UniProtKB Q6BC19 (ecto-domain of JR-FL gp160ΔCT). All samples carry mutations SOS (A501C, T605C) and E168K and N189A, and others, as denoted in the.txt files found in the MassIVE database (MSV000092416). Data were evaluated manually for each glycopeptide. A peptide was scored as true-positive when the correct b and y fragment ions were observed, along with oxonium ions corresponding to the glycan identified. The MS data was searched using the Protein Metrics “N-glycan 309 mammalian no sodium” library with sulfated glycans added manually. All charge states for a single glycopeptide were summed. The precursor mass tolerance was set at 4 ppm and 10 ppm for fragments. A 1% false discovery rate (FDR) was applied. Glycans were categorized according to the composition detected.

HexNAc(2)Hex(10+) was defined as M9Glc, HexNAc(2)Hex(9–3) was classified as M9 to M3. Any of these structures containing a fucose were categorized as FM (fucosylated mannose). HexNAc(3)Hex(5–6)X was classified as Hybrid with HexNAc(3)Hex(5–6)Fuc(1)X classified as Fhybrid. Complex glycans were classified according to the number of HexNAc subunits and the presence or absence of fucosylation. As this fragmentation method does not provide linkage information, compositional isomers are grouped. For example, a triantennary

glycan contains HexNAc(5) but so does a biantennary glycans with a bisect. Core glycans refer to truncated structures smaller than M3. M9Glc- M4 were classified as oligomannose glycans. Glycans containing at least one sialic acid were categorized as NeuAc and at least one fucose residue in the “fucose” category.

Glycans were categorized into I.D.s ranging from 1 (M9Glc) to 19 (HexNAc(6+)(F)(x)). These values were multiplied by the percentage of the corresponding glycan divided by the total glycan percentage excluding unoccupied and core glycans to give a score corresponding to the most prevalent glycan at a given site. Arithmetic score changes were then calculated from the subtraction of these scores from one sample against others, as specified.

Construction of trimer model and cognate glycans

The model representation of the JR-FL gp160 Δ CT SOS E168K+N189A trimer was constructed using SWISS-MODEL based on an existing structure of the 426c DS-SOSIP D3 trimer (pdb: 6MYY). Glycans were modelled on to this structure based on the most abundant glycoform identified from site-specific glycan analysis using WinCoot version 0.9.4.1 and PyMOL version 2.5.0. For sites that were not identified, a Man9GlcNAc2 glycan was modelled. Conditional color formatting was used to illustrate the predominant glycoforms of modeled glycans, as follows: green (high mannose), white (hybrid) and magenta (complex). Glycan score difference between clones were represented with conditional color formatting as follows: red (negative scores), white (zero score) and blue (positive scores).

Statistical analysis

All graphs were generated and analyzed using Prism (version 9.5.1).

Supporting information

S1 Fig. Densitometry analysis of various JR-FL gp160 Δ CT mutants using ImageJ. Related to [Fig 2](#). Trimer and monomer bands were normalized against JR-FL gp160 Δ CT SOS (Lane 1), while dimer bands were normalized against JR-FL gp160 Δ CT SOS NFL (Lane 2). (TIF)

S2 Fig. Analysis of additional gp160 Δ CT mutants for Env expression, gp120/gp41 processing and neutralization sensitivity. (A) JR-FL SOS parent, SOS NT1-5 (M535I+L543Q +N553S+Q567K+G588R) that also carries a D197N mutation, and SOS UNC (E168K+K510S +R511S) were analyzed by SDS-PAGE-Western blot, probed with anti-gp120 MAb (Lanes 1–3) or anti-gp41 MAb cocktail (Lanes 4–6). (B) The same samples from Part A were analyzed by BN-PAGE and probed with anti-gp120+gp41 MAb cocktail. (C) Neutralization sensitivity of JR-FL SOS gp160 Δ CT pseudoviruses with A328G (open symbols) and without A328G (filled symbols) against b12, PG16, 39F, and 15e. Neutralization assay was performed in duplicates and repeated twice. Error bar represents the standard deviation of the mean. (D) Western blot analysis of the same mutants from Part (C) by SDS-PAGE probed with anti-gp120 MAb cocktail (Lanes 1–4) or anti-gp41 MAb cocktail (Lanes 5–8), and BN-PAGE probed with anti-gp120+gp41 MAb cocktail (bottom panel). Env species are indicated by colored dots. (TIF)

S3 Fig. Effect of the DS mutation on soluble CD4 binding to JR-FL SOS gp160 Δ CT. VLP mutants from lanes 15 and 18 of Figs [2](#) and [5](#) were mixed with 4-domain soluble CD4 or PBS, then washed, lysed, and analyzed by BN-PAGE-Western blot, probed with anti-gp120+gp41 MAb cocktail. Env species are indicated by colored dots. (TIF)

S4 Fig. Western blotting analysis of gp160 Δ CT and full-length (FL) clones. (A) JR-FL WT and SOS in gp160 Δ CT and FL formats were denatured and digested with endo H and analyzed by SDS-PAGE-Western blot. Blot was probed with anti-gp120 MAb cocktail (Lanes 1–8) or anti-gp41 MAb cocktail (Lanes 9–16). (B) PC64 MRCA WT and SOS in gp160 Δ CT and FL formats were analyzed by SDS-PAGE-Western blot, probed with anti-gp120 MAb cocktail (Lanes 1–4) or anti-gp41 MAb cocktail (Lanes 5–8). (C) The same mutants from Part (B) were analyzed by BN-PAGE Western blot probed with anti-gp120+gp41 MAb cocktail. Env species are indicated by colored dots.

(TIF)

S5 Fig. BN-PAGE PGT145 shifts with and without BS³ crosslinking of JR-FL SOS E168K+N189A full length (FL). VLP bearing JR-FL SOS full length Env was incubated with PGT145 or PBS for 1h. The MAb-VLP complex was either wash with PBS (Wash out) or no washing (Leave in), followed by crosslinking with BS³. BS³ was either wash with PBS (Wash out) or no washing (Leave in), prior to electrophoresis on gel and probed with anti-gp120+gp41 MAb cocktail.

(TIF)

S6 Fig. Neutralization profile of PC64 clones. PC64 WT and SOS VLP bearing either gp160 Δ CT or full-length (FL) were incubated with MAbs, and neutralization was measured using CF2Th.CD4.CCR5 as target cells. Filled symbols represent FL and open symbol represent gp160 Δ CT. Neutralization assay was performed in duplicates and repeated twice. Error bar represents the standard deviation of the mean.

(TIF)

S7 Fig. BN-PAGE mAb shifts of key mutants with additional MAbs. Related to Fig 7. JR-FL SOS and SOS NFL I559P gp160 Δ CT mutants were analyzed in BN-PAGE shifts using selected MAbs. Duplicate blots were probed with (A) anti-gp120+gp41 MAb cocktail, followed by anti-human IgG AP conjugate, or (B) only the anti-human IgG AP conjugate.

(TIF)

S8 Fig. VLP antigenicity probed by virus capture and neutralization assays. (A) Virus capture of JR-FL gp160 Δ CT SOS E168K+N189A VLPs was evaluated using a large panel of MAbs. Values were presented as relative light unit (RLU). Virus capture assay was performed in quadruplicate and repeated at least two times. Error bars represent the standard deviation of the mean. (B) Neutralizing IC50s (μ g/ml) of the same MAbs against SOS gp160 Δ CT, WT FL and WT gp160 Δ CT. JR-FL SOS FL was non-infectious and was not included in the data analysis. Neutralization assay was performed in duplicates and repeated twice.

(TIF)

S9 Fig. Infectivity of JR-FL WT and SOS E168K+N189A PV in gp160 Δ CT and FL on CF2Th.CD4.CCR5 cells. A cutoff at 50,000 RLU (relative light unit) was indicated as the minimum readout for productive infection. Filled bars represent FL and open bars represent gp160 Δ CT. Infectivity was performed in triplicates and repeated at least twice. Error bar represents the standard deviation of the mean.

(TIF)

S10 Fig. 2G12 and CR3022 capture efficiency of various mutant VLPs. Virus capture assay was performed using (A) 2G12, or (B) CR3022 in quadruplicate and repeated at least three times. Error bars represent the standard deviation of the mean.

(TIF)

S11 Fig. ELISA of selected HIV+ plasma and 2G12 reactivity to different JR-FL gp160 Δ CT E168K+N189A VLPs. HIV+ plasma BB12, BB87, 1686 and N308, HIV- plasma 210, and 2G12 binding to JR-FL gp160 Δ CT E168K+N189A WT, SOS or SOS I559P VLP was analyzed by ELISA. VLP ELISA was repeated twice and representative data is shown.

(TIF)

S12 Fig. SDS-PAGE-Western blot of different HIV-1 Env strains bearing I559P alone or in combination with NFL. (A) VLPs expressing Q23-17 (Lanes 1–6), T250-4 (Lanes 7–12) and WITO.33 (Lanes 13–18), parent and mutant combinations were lysed and boiled in SDS/DTT, followed by digestion with endo H or PBS. Samples were analyzed in duplicate SDS-PAGE-Western blots probed with anti-gp120 MAb cocktail (top panel) or anti-gp41 MAb cocktail (bottom panels). Env species are indicated by colored dots. (B) Densitometry analysis of gp160 and gp41 band intensity for Part (A) to determine gp160:gp41 ratio.

(TIF)

S13 Fig. Glycan identity (top panels) and % fucosylated/sialylated glycan (lower panels) at each sequon position in various JR-FL gp160 Δ CT SOS E168K+N189A membrane trimers. Related to [S1 Main glycan analysis](#) and [S1 File](#) and Figs [S14–S15](#) and [11](#). Glycan maturation data of (A) viral gp160 and (B) viral gp120 derived from “parent” JR-FL gp160 Δ CT SOS E168K+N189A VLP; parent “total VLPs” of JR-FL gp160 Δ CT SOS E168K+N189A VLP preparation from (C) 2020, (D) 2021 and (E) 2023; (F) parent average of “total VLPs” of 2020, 2021 and 2023; gp160 bands derived from JR-FL mutant VLPs, namely (G) JR-FL SOS NFL, (H) SOS NFL I559P and (I) SOS NFL A433P. Glycan positions are numbered according to HxB2 strain.

(TIF)

S14 Fig. Models of glycan maturation of JR-FL gp120 monomer and membrane trimers. Related to [Fig 11](#) and [S1 Main glycan analysis](#). Models of JR-FL gp120 monomers and SOS E168K+N189A “parent” trimers (pdb: 6MYY) displaying colors that corresponds to the glycan scores. Glycan scores are colored in shades of green (high mannose) or magenta (complex). Untrimmed high mannose glycans are dark green while trimmed high mannose glycans are shown in lighter hues of green. Heavy complex glycans are shown in dark magenta, whereas smaller complex glycans are shown in lighter hues of magenta. Some glycans, rendered in gray, were not resolved in the JR-FL sample, and therefore have no score (not done, n.d.). These models were created from [S1 Main glycan analysis](#). Models include (A) Viral gp160 derived from “parent” VLP 2023; (B) Viral gp120 derived from “parent” VLP 2023; (C-E) parent “total VLPs” samples from 2020, 2021 and 2023, respectively; (F) Glycan score average of parent “total VLPs” from 2020–2023; (G) gp120 monomer (2020) made by transfecting 293T cells and purified by GN-lectin. Glycan positions are numbered according to HxB2 strain.

(TIF)

S15 Fig. Models of glycan maturation of JR-FL mutant membrane trimers. Related to [Fig 11](#) and [S1 Main glycan analysis](#). Models were created from data in [S1 Main glycan analysis](#), whereby each model represents glycan profile of gp160 bands derived from (A) SOS NFL VLP; (B) SOS NFL I559P VLP; (C) SOS NFL A433P VLP. Glycan positions are numbered according to HxB2 strain.

(TIF)

S1 Main glycan analysis. Contains 4 worksheets that summarizes glycan scores of all VLP samples (including samples from 2020 and 2021), glycan scores for average parent “total

VLPs” (2020–2023), and tabulated glycan score changes between 2 samples.
(XLSX)

S1 File. Zipped file containing 8 excel files of glycopeptide analysis of parent VLP and mutants.
(ZIP)

S1 Table. Excel file containing comparison of parent samples at variable glycan positions.
(XLSX)

Acknowledgments

We thank Bill Schief for discussions and Elise Landais for providing PC64 reagents.

Author Contributions

Conceptualization: James M. Binley.

Data curation: Tommy Tong, Alessio D'Addabbo, Jiamin Xu, Albert Nguyen, Paola Ochoa, Max Crispin.

Formal analysis: Tommy Tong, Alessio D'Addabbo, James M. Binley.

Funding acquisition: Max Crispin, James M. Binley.

Investigation: Tommy Tong, Alessio D'Addabbo, Jiamin Xu, Himanshi Chawla, Max Crispin.

Methodology: Tommy Tong, James M. Binley.

Project administration: James M. Binley.

Resources: Tommy Tong, James M. Binley.

Software: Alessio D'Addabbo, Jiamin Xu.

Supervision: Tommy Tong, Max Crispin, James M. Binley.

Validation: Tommy Tong, James M. Binley.

Visualization: Tommy Tong, Alessio D'Addabbo, Albert Nguyen, Paola Ochoa, Max Crispin.

Writing – original draft: James M. Binley.

Writing – review & editing: Tommy Tong, Jiamin Xu, James M. Binley.

References

1. Munro JB, Gorman J, Ma X, Zhou Z, Arthos J, Burton DR, et al. Conformational dynamics of single HIV-1 envelope trimers on the surface of native virions. *Science*. 2014; 346(6210):759–63. Epub 2014/10/10. <https://doi.org/10.1126/science.1254426> PMID: 25298114; PubMed Central PMCID: PMC4304640.
2. Stewart-Jones GB, Soto C, Lemmin T, Chuang GY, Druz A, Kong R, et al. Trimeric HIV-1-Env Structures Define Glycan Shields from Clades A, B, and G. *Cell*. 2016; 165(4):813–26. Epub 2016/04/27. <https://doi.org/10.1016/j.cell.2016.04.010> PMID: 27114034; PubMed Central PMCID: PMC5543418.
3. Lu M, Ma X, Castillo-Menendez LR, Gorman J, Alsahafi N, Ermel U, et al. Associating HIV-1 envelope glycoprotein structures with states on the virus observed by smFRET. *Nature*. 2019; 568(7752):415–9. Epub 2019/04/10. <https://doi.org/10.1038/s41586-019-1101-y> PMID: 30971821; PubMed Central PMCID: PMC6655592.
4. Alsahafi N, Bakouche N, Kazemi M, Richard J, Ding S, Bhattacharyya S, et al. An Asymmetric Opening of HIV-1 Envelope Mediates Antibody-Dependent Cellular Cytotoxicity. *Cell Host Microbe*. 2019; 25(4):578–87 e5. Epub 2019/04/12. <https://doi.org/10.1016/j.chom.2019.03.002> PMID: 30974085; PubMed Central PMCID: PMC6592637.

5. Julien JP, Cupo A, Sok D, Stanfield RL, Lyumkis D, Deller MC, et al. Crystal structure of a soluble cleaved HIV-1 envelope trimer. *Science*. 2013; 342(6165):1477–83. <https://doi.org/10.1126/science.1245625> PMID: 24179159; PubMed Central PMCID: PMC3886632.
6. Binley JM, Sanders RW, Clas B, Schuelke N, Master A, Guo Y, et al. A recombinant human immunodeficiency virus type 1 envelope glycoprotein complex stabilized by an intermolecular disulfide bond between the gp120 and gp41 subunits is an antigenic mimic of the trimeric virion-associated structure. *J Virol*. 2000; 74(2):627–43. <https://doi.org/10.1128/jvi.74.2.627-643.2000> PMID: 10623724
7. Sanders RW, Vesanan M, Schuelke N, Master A, Schiffner L, Kalyanaraman R, et al. Stabilization of the soluble, cleaved, trimeric form of the envelope glycoprotein complex of human immunodeficiency virus type 1. *J Virol*. 2002; 76(17):8875–89. <https://doi.org/10.1128/jvi.76.17.8875-8889.2002> PMID: 12163607.
8. Kong L, He L, de Val N, Vora N, Morris CD, Azadnia P, et al. Uncleaved prefusion-optimized gp140 trimers derived from analysis of HIV-1 envelope metastability. *Nat Commun*. 2016; 7:12040. Epub 20160628. <https://doi.org/10.1038/ncomms12040> PMID: 27349805; PubMed Central PMCID: PMC4931249.
9. Sharma SK, de Val N, Bale S, Guenaga J, Tran K, Feng Y, et al. Cleavage-independent HIV-1 Env trimers engineered as soluble native spike mimetics for vaccine design. *Cell Rep*. 2015; 11(4):539–50. Epub 2015/04/22. <https://doi.org/10.1016/j.celrep.2015.03.047> PMID: 25892233; PubMed Central PMCID: PMC4637274.
10. Aldon Y, McKay PF, Allen J, Ozorowski G, Felfodine Levai R, Tolazzi M, et al. Rational Design of DNA-Expressed Stabilized Native-Like HIV-1 Envelope Trimers. *Cell Rep*. 2018; 24(12):3324–38 e5. Epub 2018/09/21. <https://doi.org/10.1016/j.celrep.2018.08.051> PMID: 30232012; PubMed Central PMCID: PMC6167709.
11. Kwon YD, Pancera M, Acharya P, Georgiev IS, Crooks ET, Gorman J, et al. Crystal structure, conformational fixation and entry-related interactions of mature ligand-free HIV-1 Env. *Nat Struct Mol Biol*. 2015; 22(7):522–31. Epub 2015/06/23. <https://doi.org/10.1038/nsmb.3051> PMID: 26098315; PubMed Central PMCID: PMC4706170.
12. de Taeye SW, Moore JP, Sanders RW. HIV-1 Envelope Trimer Design and Immunization Strategies To Induce Broadly Neutralizing Antibodies. *Trends Immunol*. 2016; 37(3):221–32. <https://doi.org/10.1016/j.it.2016.01.007> PMID: 26869204.
13. Joyce MG, Georgiev IS, Yang Y, Druz A, Geng H, Chuang GY, et al. Soluble Prefusion Closed DS-SOSIP.664-Env Trimers of Diverse HIV-1 Strains. *Cell Rep*. 2017; 21(10):2992–3002. Epub 2017/12/07. <https://doi.org/10.1016/j.celrep.2017.11.016> PMID: 29212041.
14. Rawi R, Rutten L, Lai YT, Olia AS, Blokland S, Juraszek J, et al. Automated Design by Structure-Based Stabilization and Consensus Repair to Achieve Prefusion-Closed Envelope Trimers in a Wide Variety of HIV Strains. *Cell Rep*. 2020; 33(8):108432. Epub 2020/11/26. <https://doi.org/10.1016/j.celrep.2020.108432> PMID: 33238130; PubMed Central PMCID: PMC7714614.
15. Guenaga J, Dubrovskaya V, de Val N, Sharma SK, Carrette B, Ward AB, et al. Structure-Guided Redesign Increases the Propensity of HIV Env To Generate Highly Stable Soluble Trimers. *J Virol*. 2015; 90(6):2806–17. Epub 2016/01/01. <https://doi.org/10.1128/JVI.02652-15> PMID: 26719252; PubMed Central PMCID: PMC4810649.
16. Guenaga J, Garces F, de Val N, Stanfield RL, Dubrovskaya V, Higgins B, et al. Glycine Substitution at Helix-to-Coil Transitions Facilitates the Structural Determination of a Stabilized Subtype C HIV Envelope Glycoprotein. *Immunity*. 2017; 46(5):792–803 e3. Epub 2017/05/18. <https://doi.org/10.1016/j.immuni.2017.04.014> PMID: 28514686; PubMed Central PMCID: PMC5439057.
17. Dey AK, David KB, Ray N, Ketas TJ, Klasse PJ, Doms RW, et al. N-terminal substitutions in HIV-1 gp41 reduce the expression of non-trimeric envelope glycoproteins on the virus. *Virology*. 2008; 372(1):187–200. <https://doi.org/10.1016/j.virol.2007.10.018> PMID: 18031785; PubMed Central PMCID: PMC2317825.
18. Dey AK, David KB, Klasse PJ, Moore JP. Specific amino acids in the N-terminus of the gp41 ectodomain contribute to the stabilization of a soluble, cleaved gp140 envelope glycoprotein from human immunodeficiency virus type 1. *Virology*. 2007; 360(1):199–208. <https://doi.org/10.1016/j.virol.2006.09.046> PMID: 17092531; PubMed Central PMCID: PMC1857345.
19. Rutten L, Lai YT, Blokland S, Truan D, Bisschop IJM, Strokappe NM, et al. A Universal Approach to Optimize the Folding and Stability of Prefusion-Closed HIV-1 Envelope Trimers. *Cell Rep*. 2018; 23(2):584–95. Epub 2018/04/12. <https://doi.org/10.1016/j.celrep.2018.03.061> PMID: 29642014; PubMed Central PMCID: PMC6010203.
20. Beltran-Pavez C, Bontjer I, Gonzalez N, Pernas M, Merino-Mansilla A, Olvera A, et al. Potent Induction of Envelope-Specific Antibody Responses by Virus-Like Particle Immunogens Based on HIV-1 Envelopes from Patients with Early Broadly Neutralizing Responses. *J Virol*. 2022; 96(1):e0134321. Epub

20211020. <https://doi.org/10.1128/JVI.01343-21> PMID: 34668778; PubMed Central PMCID: PMC8754226.
21. Medina-Ramirez M, Sanders RW, Klasse PJ. Targeting B-cell germlines and focusing affinity maturation: the next hurdles in HIV-1-vaccine development? *Expert Rev Vaccines*. 2014; 13(4):449–52. <https://doi.org/10.1586/14760584.2014.894469> PMID: 24606603; PubMed Central PMCID: PMC4141483.
22. Crooks ET, Almanza F, D'Addabbo A, Duggan E, Zhang J, Wagh K, et al. Engineering well-expressed, V2-immunofocusing HIV-1 envelope glycoprotein membrane trimers for use in heterologous prime-boost vaccine regimens. *PLoS Pathog*. 2021; 17(10):e1009807. Epub 2021/10/23. <https://doi.org/10.1371/journal.ppat.1009807> PMID: 34679128; PubMed Central PMCID: PMC8565784.
23. Nguyen HT, Qualizza A, Anang S, Zhao M, Zou S, Zhou R, et al. Functional and Highly Cross-Linkable HIV-1 Envelope Glycoproteins Enriched in a Pretriggered Conformation. *J Virol*. 2022; 96(8):e0166821. Epub 20220328. <https://doi.org/10.1128/jvi.01668-21> PMID: 35343783; PubMed Central PMCID: PMC9044932.
24. Crooks ET, Moore PL, Franti M, Cayanan CS, Zhu P, Jiang P, et al. A comparative immunogenicity study of HIV-1 virus-like particles bearing various forms of envelope proteins, particles bearing no envelope and soluble monomeric gp120. *Virology*. 2007; 366(2):245–62. <https://doi.org/10.1016/j.virol.2007.04.033> PMID: 17580087.
25. Crooks ET, Osawa K, Tong T, Grimley SL, Dai YD, Whalen RG, et al. Effects of partially dismantling the CD4 binding site glycan fence of HIV-1 Envelope glycoprotein trimers on neutralizing antibody induction. *Virology*. 2017; 505:193–209. <https://doi.org/10.1016/j.virol.2017.02.024> PMID: 28279830.
26. Crooks ET, Tong T, Chakrabarti B, Narayan K, Georgiev IS, Menis S, et al. Vaccine-Elicited Tier 2 HIV-1 Neutralizing Antibodies Bind to Quaternary Epitopes Involving Glycan-Deficient Patches Proximal to the CD4 Binding Site. *PLoS Pathog*. 2015; 11(5):e1004932. <https://doi.org/10.1371/journal.ppat.1004932> PMID: 26023780.
27. Zhang S, Wang K, Wang WL, Nguyen HT, Chen S, Lu M, et al. Asymmetric Structures and Conformational Plasticity of the Uncleaved Full-Length Human Immunodeficiency Virus Envelope Glycoprotein Trimer. *J Virol*. 2021; 95(24):e0052921. Epub 20210922. <https://doi.org/10.1128/JVI.00529-21> PMID: 34549974; PubMed Central PMCID: PMC8610584.
28. McCaul N, Quandt M, Bontjer I, van Zadelhoff G, Land A, Crooks ET, et al. Intramolecular quality control: HIV-1 envelope gp160 signal-peptide cleavage as a functional folding checkpoint. *Cell Rep*. 2021; 36(9):109646. Epub 2021/09/02. <https://doi.org/10.1016/j.celrep.2021.109646> PMID: 34469718.
29. Haim H, Salas I, Sodroski J. Proteolytic processing of the human immunodeficiency virus envelope glycoprotein precursor decreases conformational flexibility. *J Virol*. 2013; 87(3):1884–9. <https://doi.org/10.1128/JVI.02765-12> PMID: 23175369.
30. Moore PL, Crooks ET, Porter L, Zhu P, Cayanan CS, Grise H, et al. Nature of nonfunctional envelope proteins on the surface of human immunodeficiency virus type 1. *J Virol*. 2006; 80(5):2515–28. <https://doi.org/10.1128/JVI.80.5.2515-2528.2006> PMID: 16474158.
31. Castillo-Menendez LR, Nguyen HT, Sodroski J. Conformational Differences between Functional Human Immunodeficiency Virus Envelope Glycoprotein Trimers and Stabilized Soluble Trimers. *J Virol*. 2019; 93(3). Epub 20190117. <https://doi.org/10.1128/JVI.01709-18> PMID: 30429345; PubMed Central PMCID: PMC6340038.
32. Pancera M, Wyatt R. Selective recognition of oligomeric HIV-1 primary isolate envelope glycoproteins by potently neutralizing ligands requires efficient precursor cleavage. *Virology*. 2005; 332(1):145–56. <https://doi.org/10.1016/j.virol.2004.10.042> PMID: 15661147.
33. Castillo-Menendez LR, Witt K, Espy N, Princiotti A, Madani N, Pacheco B, et al. Comparison of Uncleaved and Mature Human Immunodeficiency Virus Membrane Envelope Glycoprotein Trimers. *J Virol*. 2018; 92(12). Epub 20180529. <https://doi.org/10.1128/JVI.00277-18> PMID: 29618643; PubMed Central PMCID: PMC5974486.
34. Zhang S, Nguyen HT, Ding H, Wang J, Zou S, Liu L, et al. Dual Pathways of Human Immunodeficiency Virus Type 1 Envelope Glycoprotein Trafficking Modulate the Selective Exclusion of Uncleaved Oligomers from Virions. *J Virol*. 2021; 95(3). Epub 20210113. <https://doi.org/10.1128/JVI.01369-20> PMID: 33148792; PubMed Central PMCID: PMC7925103.
35. Stadtmauer BM, Bridges MD, Dam KM, Lerch MT, Huey-Tubman KE, Hubbell WL, et al. DEER Spectroscopy Measurements Reveal Multiple Conformations of HIV-1 SOSIP Envelopes that Show Similarities with Envelopes on Native Virions. *Immunity*. 2018; 49(2):235–46 e4. Epub 20180731. <https://doi.org/10.1016/j.immuni.2018.06.017> PMID: 30076100; PubMed Central PMCID: PMC6104740.
36. Nguyen HT, Alsahafi N, Finzi A, Sodroski JG. Effects of the SOS (A501C/T605C) and DS (I201C/A433C) Disulfide Bonds on HIV-1 Membrane Envelope Glycoprotein Conformation and Function. *J*

- Virol. 2019; 93(12). Epub 20190529. <https://doi.org/10.1128/JVI.00304-19> PMID: 30944182; PubMed Central PMCID: PMC6613753.
37. Salimi H, Johnson J, Flores MG, Zhang MS, O'Malley Y, Houtman JC, et al. The lipid membrane of HIV-1 stabilizes the viral envelope glycoproteins and modulates their sensitivity to antibody neutralization. *J Biol Chem.* 2020; 295(2):348–62. Epub 20191122. <https://doi.org/10.1074/jbc.RA119.009481> PMID: 31757809; PubMed Central PMCID: PMC6956520.
38. Alsahafi N, Debbeche O, Sodroski J, Finzi A. Effects of the I559P gp41 change on the conformation and function of the human immunodeficiency virus (HIV-1) membrane envelope glycoprotein trimer. *PLoS One.* 2015; 10(4):e0122111. Epub 2015/04/08. <https://doi.org/10.1371/journal.pone.0122111> PMID: 25849367; PubMed Central PMCID: PMC4388519.
39. Kesavardhana S, Varadarajan R. Stabilizing the native trimer of HIV-1 Env by destabilizing the heterodimeric interface of the gp41 postfusion six-helix bundle. *J Virol.* 2014; 88(17):9590–604. Epub 20140611. <https://doi.org/10.1128/JVI.00494-14> PMID: 24920800; PubMed Central PMCID: PMC4136328.
40. Alsahafi N, Anand SP, Castillo-Menendez L, Verly MM, Medjahed H, Prevost J, et al. SOSIP changes affect human immunodeficiency virus (HIV-1) envelope glycoprotein conformation and CD4 engagement. *J Virol.* 2018. Epub 2018/07/20. <https://doi.org/10.1128/JVI.01080-18> PMID: 30021898; PubMed Central PMCID: PMC6146791.
41. Cale EM, Driscoll JI, Lee M, Gorman J, Zhou T, Lu M, et al. Antigenic analysis of the HIV-1 envelope trimer implies small differences between structural states 1 and 2. *J Biol Chem.* 2022; 298(4):101819. Epub 20220310. <https://doi.org/10.1016/j.jbc.2022.101819> PMID: 35283191; PubMed Central PMCID: PMC9006658.
42. Lu M, Ma X, Reichard N, Terry DS, Arthos J, Smith AB 3rd, et al. Shedding-Resistant HIV-1 Envelope Glycoproteins Adopt Downstream Conformations That Remain Responsive to Conformation-Preferring Ligands. *J Virol.* 2020; 94(17). Epub 20200817. <https://doi.org/10.1128/JVI.00597-20> PMID: 32522853; PubMed Central PMCID: PMC7431789.
43. Upadhyay C, Feyznezhad R, Yang W, Zhang H, Zolla-Pazner S, Hioe CE. Alterations of HIV-1 envelope phenotype and antibody-mediated neutralization by signal peptide mutations. *PLoS Pathog.* 2018; 14(1):e1006812. Epub 20180125. <https://doi.org/10.1371/journal.ppat.1006812> PMID: 29370305; PubMed Central PMCID: PMC5800646.
44. Upadhyay C, Feyznezhad R, Cao L, Chan KW, Liu K, Yang W, et al. Signal peptide of HIV-1 envelope modulates glycosylation impacting exposure of V1V2 and other epitopes. *PLoS Pathog.* 2020; 16(12): e1009185. Epub 20201228. <https://doi.org/10.1371/journal.ppat.1009185> PMID: 33370382; PubMed Central PMCID: PMC7793277.
45. Pfeiffer T, Pisch T, Devitt G, Holtkotte D, Bosch V. Effects of signal peptide exchange on HIV-1 glycoprotein expression and viral infectivity in mammalian cells. *FEBS Lett.* 2006; 580(15):3775–8. Epub 20060609. <https://doi.org/10.1016/j.febslet.2006.05.070> PMID: 16777098.
46. Crooks ET, Grimley SL, Cully M, Osawa K, Dekkers G, Saunders K, et al. Glycoengineering HIV-1 Env creates 'supercharged' and 'hybrid' glycans to increase neutralizing antibody potency, breadth and saturation. *PLoS Pathog.* 2018; 14(5):e1007024. Epub 2018/05/03. <https://doi.org/10.1371/journal.ppat.1007024> PMID: 29718999; PubMed Central PMCID: PMC5951585.
47. Rauch S, Jasny E, Schmidt KE, Petsch B. New Vaccine Technologies to Combat Outbreak Situations. *Front Immunol.* 2018; 9:1963. Epub 20180919. <https://doi.org/10.3389/fimmu.2018.01963> PMID: 30283434; PubMed Central PMCID: PMC6156540.
48. Pardi N, Hogan MJ, Porter FW, Weissman D. mRNA vaccines—a new era in vaccinology. *Nat Rev Drug Discov.* 2018; 17(4):261–79. Epub 20180112. <https://doi.org/10.1038/nrd.2017.243> PMID: 29326426; PubMed Central PMCID: PMC5906799.
49. Baden LR, El Sahly HM, Essink B, Kotloff K, Frey S, Novak R, et al. Efficacy and Safety of the mRNA-1273 SARS-CoV-2 Vaccine. *N Engl J Med.* 2021; 384(5):403–16. Epub 20201230. <https://doi.org/10.1056/NEJMoa2035389> PMID: 33378609; PubMed Central PMCID: PMC7787219.
50. Polack FP, Thomas SJ, Kitchin N, Absalon J, Gurtman A, Lockhart S, et al. Safety and Efficacy of the BNT162b2 mRNA Covid-19 Vaccine. *N Engl J Med.* 2020; 383(27):2603–15. Epub 2020/12/11. <https://doi.org/10.1056/NEJMoa2034577> PMID: 33301246; PubMed Central PMCID: PMC7745181.
51. Zhang P, Narayanan E, Liu Q, Tsybovsky Y, Boswell K, Ding S, et al. A multiclade env-gag VLP mRNA vaccine elicits tier-2 HIV-1-neutralizing antibodies and reduces the risk of heterologous SHIV infection in macaques. *Nat Med.* 2021; 27(12):2234–45. Epub 20211209. <https://doi.org/10.1038/s41591-021-01574-5> PMID: 34887575.
52. Mu Z, Wiehe K, Saunders KO, Henderson R, Cain DW, Parks R, et al. mRNA-encoded HIV-1 Env trimer ferritin nanoparticles induce monoclonal antibodies that neutralize heterologous HIV-1 isolates in mice.

- Cell Rep. 2022; 38(11):110514. <https://doi.org/10.1016/j.celrep.2022.110514> PMID: 35294883; PubMed Central PMCID: PMC8922439.
53. Aldon Y, McKay PF, Moreno Herrero J, Vogel AB, Levai R, Maisonnasse P, et al. Immunogenicity of stabilized HIV-1 Env trimers delivered by self-amplifying mRNA. *Mol Ther Nucleic Acids*. 2021; 25:483–93. Epub 20210624. <https://doi.org/10.1016/j.omtn.2021.06.008> PMID: 34589271; PubMed Central PMCID: PMC8463288.
54. Saunders KO, Pardi N, Parks R, Santra S, Mu Z, Sutherland L, et al. Lipid nanoparticle encapsulated nucleoside-modified mRNA vaccines elicit polyfunctional HIV-1 antibodies comparable to proteins in nonhuman primates. *NPJ Vaccines*. 2021; 6(1):50. Epub 2021/04/11. <https://doi.org/10.1038/s41541-021-00307-6> PMID: 33837212; PubMed Central PMCID: PMC8035178.
55. Melzi E, Willis JR, Ma KM, Lin YC, Kratochvil S, Berndsen ZT, et al. Membrane-bound mRNA immunogens lower the threshold to activate HIV Env V2 apex-directed broadly neutralizing B cell precursors in humanized mice. *Immunity*. 2022; 55(11):2168–86 e6. Epub 20220929. <https://doi.org/10.1016/j.immuni.2022.09.003> PMID: 36179690; PubMed Central PMCID: PMC9671093.
56. Pardi N, Hogan MJ, Naradikian MS, Parkhouse K, Cain DW, Jones L, et al. Nucleoside-modified mRNA vaccines induce potent T follicular helper and germinal center B cell responses. *J Exp Med*. 2018; 215(6):1571–88. Epub 2018/05/10. <https://doi.org/10.1084/jem.20171450> PMID: 29739835; PubMed Central PMCID: PMC5987916.
57. Gonelli CA, King HAD, Mackenzie C, Sonza S, Center RJ, Purcell DFJ. Immunogenicity of HIV-1-Based Virus-Like Particles with Increased Incorporation and Stability of Membrane-Bound Env. *Vaccines (Basel)*. 2021; 9(3). Epub 20210310. <https://doi.org/10.3390/vaccines9030239> PMID: 33801906; PubMed Central PMCID: PMC8002006.
58. Steichen JM, Kulp DW, Tokatlian T, Escolano A, Dosenovic P, Stanfield RL, et al. HIV Vaccine Design to Target Germine Precursors of Glycan-Dependent Broadly Neutralizing Antibodies. *Immunity*. 2016; 45(3):483–96. <https://doi.org/10.1016/j.immuni.2016.08.016> PMID: 27617678; PubMed Central PMCID: PMC5040827.
59. Martinez DR, Schafer A, Leist SR, De la Cruz G, West A, Atochina-Vasserman EN, et al. Chimeric spike mRNA vaccines protect against Sarbecovirus challenge in mice. *Science*. 2021; 373(6558):991–8. Epub 20210622. <https://doi.org/10.1126/science.abi4506> PMID: 34214046; PubMed Central PMCID: PMC8899822.
60. Binley JM, Cayanan CS, Wiley C, Schulke N, Olson WC, Burton DR. Redox-triggered infection by disulfide-shackled human immunodeficiency virus type 1 pseudovirions. *J Virol*. 2003; 77(10):5678–84. <https://doi.org/10.1128/JVI.77.10.5678-5684.2003> PMID: 12719560.
61. Yang L, Sharma SK, Cottrell C, Guenaga J, Tran K, Wilson R, et al. Structure-Guided Redesign Improves NFL HIV Env Trimer Integrity and Identifies an Inter-Protomer Disulfide Permitting Post-Expression Cleavage. *Front Immunol*. 2018; 9:1631. Epub 20180717. <https://doi.org/10.3389/fimmu.2018.01631> PMID: 30065725; PubMed Central PMCID: PMC6056610.
62. Cale EM, Gorman J, Radakovich NA, Crooks ET, Osawa K, Tong T, et al. Virus-like Particles Identify an HIV V1V2 Apex-Binding Neutralizing Antibody that Lacks a Protruding Loop. *Immunity*. 2017; 46(5):777–91 e10. <https://doi.org/10.1016/j.immuni.2017.04.011> PMID: 28514685.
63. Doores KJ, Bonomelli C, Harvey DJ, Vasiljevic S, Dwek RA, Burton DR, et al. Envelope glycans of immunodeficiency virions are almost entirely oligomannose antigens. *Proc Natl Acad Sci U S A*. 2010; 107(31):13800–5. Epub 2010/07/21. <https://doi.org/10.1073/pnas.1006498107> [pii] PMID: 20643940.
64. Crooks ET, Tong T, Osawa K, Binley JM. Enzyme digests eliminate nonfunctional Env from HIV-1 particle surfaces, leaving native Env trimers intact and viral infectivity unaffected. *J Virol*. 2011; 85(12):5825–39. <https://doi.org/10.1128/JVI.00154-11> PMID: 21471242; PubMed Central PMCID: PMC3126298.
65. Schiffner T, Kong L, Duncan CJ, Back JW, Benschop JJ, Shen X, et al. Immune focusing and enhanced neutralization induced by HIV-1 gp140 chemical cross-linking. *J Virol*. 2013; 87(18):10163–72. <https://doi.org/10.1128/JVI.01161-13> PMID: 23843636; PubMed Central PMCID: PMC3754013.
66. Tong T, Osawa K, Robinson JE, Crooks ET, Binley JM. Topological Analysis of HIV-1 Glycoproteins Expressed in situ on Virus Surfaces Reveals Tighter Packing but Greater Conformational Flexibility Compared to Soluble Gp120. *J Virol*. 2013. <https://doi.org/10.1128/JVI.01145-13> PMID: 23740975.
67. Wyss S, Dimitrov AS, Baribaud F, Edwards TG, Blumenthal R, Hoxie JA. Regulation of human immunodeficiency virus type 1 envelope glycoprotein fusion by a membrane-interactive domain in the gp41 cytoplasmic tail. *J Virol*. 2005; 79(19):12231–41. <https://doi.org/10.1128/JVI.79.19.12231-12241.2005> PMID: 16160149.
68. Edwards TG, Wyss S, Reeves JD, Zolla-Pazner S, Hoxie JA, Doms RW, et al. Truncation of the cytoplasmic domain induces exposure of conserved regions in the ectodomain of human immunodeficiency

- virus type 1 envelope protein. *J Virol.* 2002; 76(6):2683–91. <https://doi.org/10.1128/jvi.76.6.2683-2691.2002> PMID: 11861835.
69. Landais E, Huang X, Havenar-Daughton C, Murrell B, Price MA, Wickramasinghe L, et al. Broadly Neutralizing Antibody Responses in a Large Longitudinal Sub-Saharan HIV Primary Infection Cohort. *PLoS Pathog.* 2016; 12(1):e1005369. <https://doi.org/10.1371/journal.ppat.1005369> PMID: 26766578; PubMed Central PMCID: PMC4713061.
70. Herschhorn A, Gu C, Moraca F, Ma X, Farrell M, Smith AB 3rd, et al. The beta₂₀-beta₂₁ of gp120 is a regulatory switch for HIV-1 Env conformational transitions. *Nat Commun.* 2017; 8(1):1049. Epub 2017/10/21. <https://doi.org/10.1038/s41467-017-01119-w> PMID: 29051495; PubMed Central PMCID: PMC5648922.
71. Binley JM, Lybarger EA, Crooks ET, Seaman MS, Gray E, Davis KL, et al. Profiling the specificity of neutralizing antibodies in a large panel of plasmas from patients chronically infected with human immunodeficiency virus type 1 subtypes B and C. *Journal of virology.* 2008; 82(23):11651–68. Epub 2008/09/26. <https://doi.org/10.1128/JVI.01762-08> PMID: 18815292; PubMed Central PMCID: PMC2583680.
72. Struwe WB, Chertova E, Allen JD, Seabright GE, Watanabe Y, Harvey DJ, et al. Site-Specific Glycosylation of Virion-Derived HIV-1 Env Is Mimicked by a Soluble Trimeric Immunogen. *Cell Rep.* 2018; 24(8):1958–66 e5. Epub 2018/08/23. <https://doi.org/10.1016/j.celrep.2018.07.080> PMID: 30134158; PubMed Central PMCID: PMC6113929.
73. Behrens AJ, Vasiljevic S, Pritchard LK, Harvey DJ, Andev RS, Krumm SA, et al. Composition and Antigenic Effects of Individual Glycan Sites of a Trimeric HIV-1 Envelope Glycoprotein. *Cell Rep.* 2016; 14(11):2695–706. <https://doi.org/10.1016/j.celrep.2016.02.058> PMID: 26972002; PubMed Central PMCID: PMC4805854.
74. Cao L, Pauthner M, Andrabi R, Rantalainen K, Berndsen Z, Diedrich JK, et al. Differential processing of HIV envelope glycans on the virus and soluble recombinant trimer. *Nat Commun.* 2018; 9(1):3693. Epub 2018/09/14. <https://doi.org/10.1038/s41467-018-06121-4> PMID: 30209313; PubMed Central PMCID: PMC6135743.
75. Wrapp D, Mu Z, Thakur B, Janowska K, Ajayi O, Barr M, et al. Structure-Based Stabilization of SOSIP Env Enhances Recombinant Ectodomain Durability and Yield. *J Virol.* 2023; 97(1):e0167322. Epub 2023/01/12. <https://doi.org/10.1128/jvi.01673-22> PMID: 36633409; PubMed Central PMCID: PMC9888283.
76. Panico M, Bouche L, Binet D, O'Connor MJ, Rahman D, Pang PC, et al. Mapping the complete glycoproteome of virion-derived HIV-1 gp120 provides insights into broadly neutralizing antibody binding. *Sci Rep.* 2016; 6:32956. Epub 2016/09/09. <https://doi.org/10.1038/srep32956> PMID: 27604319; PubMed Central PMCID: PMC5015092.
77. Pritchard LK, Harvey DJ, Bonomelli C, Crispin M, Doores KJ. Cell- and Protein-Directed Glycosylation of Native Cleaved HIV-1 Envelope. *J Virol.* 2015; 89(17):8932–44. <https://doi.org/10.1128/JVI.01190-15> PMID: 26085151; PubMed Central PMCID: PMC4524065.
78. Welbourn S, Chakraborty S, Yang JE, Gleinrich AS, Gangadhara S, Khan S, et al. A neutralizing antibody target in early HIV-1 infection was recapitulated in rhesus macaques immunized with the transmitted/founder envelope sequence. *PLoS Pathog.* 2022; 18(5):e1010488. Epub 2022/05/03. <https://doi.org/10.1371/journal.ppat.1010488> PMID: 35503780; PubMed Central PMCID: PMC9106183.
79. Derking R, Allen JD, Cottrell CA, Sliepen K, Seabright GE, Lee WH, et al. Enhancing glycan occupancy of soluble HIV-1 envelope trimers to mimic the native viral spike. *Cell Rep.* 2021; 35(1):108933. Epub 2021/04/08. <https://doi.org/10.1016/j.celrep.2021.108933> PMID: 33826885.
80. McCoy LE, van Gils MJ, Ozorowski G, Messmer T, Briney B, Voss JE, et al. Holes in the Glycan Shield of the Native HIV Envelope Are a Target of Trimer-Elicited Neutralizing Antibodies. *Cell Rep.* 2016; 16(9):2327–38. <https://doi.org/10.1016/j.celrep.2016.07.074> PMID: 27545891; PubMed Central PMCID: PMC5007210.
81. Blish CA, Nguyen MA, Overbaugh J. Enhancing exposure of HIV-1 neutralization epitopes through mutations in gp41. *PLoS Med.* 2008; 5(1):e9. <https://doi.org/10.1371/journal.pmed.0050009> PMID: 18177204.
82. Zhang P, Kwon AL, Guzzo C, Liu Q, Schmeisser H, Miao H, et al. Functional Anatomy of the Trimer Apex Reveals Key Hydrophobic Constraints That Maintain the HIV-1 Envelope Spike in a Closed State. *mBio.* 2021; 12(2). Epub 2021/04/01. <https://doi.org/10.1128/mBio.00090-21> PMID: 33785631; PubMed Central PMCID: PMC8092198.
83. Earl PL, Moss B, Doms RW. Folding, interaction with GRP78-BiP, assembly, and transport of the human immunodeficiency virus type 1 envelope protein. *J Virol.* 1991; 65(4):2047–55. <https://doi.org/10.1128/JVI.65.4.2047-2055.1991> PMID: 1900540

84. Tong T, Crooks ET, Osawa K, Robinson JE, Barnes M, Apetrei C, et al. Multi-parameter exploration of HIV-1 virus-like particles as neutralizing antibody immunogens in guinea pigs, rabbits and macaques. *Virology*. 2014; 456–457:55–69. <https://doi.org/10.1016/j.virol.2014.03.015> PMID: 24889225.
85. Chen J, Kovacs JM, Peng H, Rits-Volloch S, Lu J, Park D, et al. HIV-1 ENVELOPE. Effect of the cytoplasmic domain on antigenic characteristics of HIV-1 envelope glycoprotein. *Science*. 2015; 349(6244):191–5. <https://doi.org/10.1126/science.aaa9804> PMID: 26113642; PubMed Central PMCID: PMC4701381.
86. van Schooten J, van Haaren MM, Li H, McCoy LE, Havenar-Daughton C, Cottrell CA, et al. Antibody responses induced by SHIV infection are more focused than those induced by soluble native HIV-1 envelope trimers in non-human primates. *PLoS Pathog*. 2021; 17(8):e1009736. Epub 20210825. <https://doi.org/10.1371/journal.ppat.1009736> PMID: 34432859; PubMed Central PMCID: PMC8423243.
87. Wagh K, Kreider EF, Li Y, Barbian HJ, Learn GH, Giorgi E, et al. Completeness of HIV-1 Envelope Glycan Shield at Transmission Determines Neutralization Breadth. *Cell Rep*. 2018; 25(4):893–908 e7. Epub 2018/10/26. <https://doi.org/10.1016/j.celrep.2018.09.087> PMID: 30355496.
88. Roark RS, Li H, Williams WB, Chug H, Mason RD, Gorman J, et al. Recapitulation of HIV-1 Env-antibody coevolution in macaques leading to neutralization breadth. *Science*. 2021; 371(6525). Epub 20201119. <https://doi.org/10.1126/science.abd2638> PMID: 33214287; PubMed Central PMCID: PMC8040783.
89. Xu K, Acharya P, Kong R, Cheng C, Chuang GY, Liu K, et al. Epitope-based vaccine design yields fusion peptide-directed antibodies that neutralize diverse strains of HIV-1. *Nat Med*. 2018; 24(6):857–67. Epub 2018/06/06. <https://doi.org/10.1038/s41591-018-0042-6> PMID: 29867235.
90. Crooks ET, Moore PL, Richman D, Robinson J, Crooks JA, Franti M, et al. Characterizing anti-HIV monoclonal antibodies and immune sera by defining the mechanism of neutralization. *Hum Antibodies*. 2005; 14(3–4):101–13. Epub 2006/05/25. PMID: 16720980; PubMed Central PMCID: PMC2630880.
91. Nyambi PN, Gorny MK, Bastiani L, van der Groen G, Williams C, Zolla-Pazner S. Mapping of epitopes exposed on intact human immunodeficiency virus type 1 (HIV-1) virions: a new strategy for studying the immunologic relatedness of HIV-1. *J Virol*. 1998; 72(11):9384–91. <https://doi.org/10.1128/JVI.72.11.9384-9391.1998> PMID: 9765494.
92. Poignard P, Moulard M, Golez E, Vivona V, Franti M, Venturini S, et al. Heterogeneity of envelope molecules expressed on primary human immunodeficiency virus type 1 particles as probed by the binding of neutralizing and nonneutralizing antibodies. *J Virol*. 2003; 77(1):353–65. <https://doi.org/10.1128/JVI.77.1.353-365.2003> PMID: 12477840.
93. Tong T, Crooks ET, Osawa K, Binley JM. HIV-1 virus-like particles bearing pure env trimers expose neutralizing epitopes but occlude nonneutralizing epitopes. *J Virol*. 2012; 86(7):3574–87. <https://doi.org/10.1128/JVI.06938-11> PMID: 22301141; PubMed Central PMCID: PMC3302546.